63_3_5

405 046

WADD TR 61-42
Part III

STUDY OF ULTRASONIC TECHNIQUES FOR THE NONDESTRUCTIVE MEASUREMENT OF RESIDUAL STRESS

405 046

TECHNICAL DOCUMENTARY REPORT NO. WADD TR 61-42, Pt. III
May 1963

Directorate of Materials and Processes
Aeronautical Systems Division
Air Force Systems Command
Wright-Patterson Air Force Base, Ohio

Project No. 7360, Task No. 73606

(Prepared under Contract No. AF 33(616)-7058
by the Midwest Research Institute, Kansas City, Missouri;
Fred R. Rollins, Jr., and Peter Waldow, authors.)

NOTICES

When Government drawings, specifications, or other data are used for any purpose other than in connection with a definitely related Government procurement operation, the United States Government thereby incurs no responsibility nor any obligation whatsoever; and the fact that the Government may have formulated, furnished, or in any way supplied the said drawings, specifications, or other data, is not to be regarded by implication or otherwise as in any manner licensing the holder or any other person or corporation, or conveying any rights or permission to manufacture, use, or sell any patented invention that may in any way be related thereto.

Qualified requesters may obtain copies of this report from the Armed Services Technical Information Agency, (ASTIA), Arlington Hall Station, Arlington 12, Virginia.

This report has been released to the Office of Technical Services, U. S. Department of Commerce, Washington 25, D.C., for sale to the general public.

Copies of this report should not be returned to the Aeronautical Systems Division unless return is required by security considerations, contractual obligations, or notice on a specific document.

FOREWORD

This report was prepared by Midwest Research Institute under USAF Contract No. AF 33(616)-7058. The contract was initiated under Project No. 7360, "The Chemistry and Physics of Materials," Task No. 73606, "Nondestructive Methods." The work was administered under the Directorate of Materials and Processes, Deputy for Technology, Aeronautical Systems Division, with Mr. Harold Kamm acting as project engineer.

This report covers work conducted from 1 February 1962 to 31 January 1963.

The work was performed under the direction of Mr. Fred R. Rollins, Jr. Other personnel directly involved in prosecution of the research have been Messrs. Paul Gutshall, Lyle Taylor, L. S. Srinath, and Peter Waldow.

ABSTRACT

The theoretical and experimental investigation of ultrasonic beam interaction in solid materials has been continued. Intersection of pulsed beams (3 - 15 mc/s) under "resonant" conditions reveals that interaction does occur in many materials. A theoretically predicted third beam is generated at the "point" of intersection and has been experimentally observed in samples of fused silica, polycrystalline aluminum, and polycrystalline magnesium. A potential method of three-dimensional stress analysis is discussed. An optical system for studying beam interaction in transparent solids is also described.

This technical report has been reviewed and is approved.

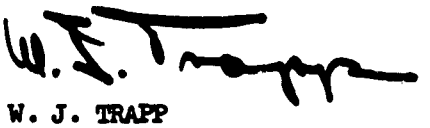

W. J. TRAPP
Chief, Strength and Dynamics Branch
Metals and Ceramics Laboratory
Directorate of Materials and Processes

TABLE OF CONTENTS

LIST OF ILLUSTRATIONS

LIST OF ILLUSTRATIONS

LIST OF ILLUSTRATIONS (Concluded)

LIST OF TABLES

I. INTRODUCTION

During the past several years Midwest Research Institute has been engaged in a study of certain stress-dependent aspects of ultrasonic propagation in solid materials. A thorough understanding of these stress-dependent properties should greatly facilitate the ultimate use of ultrasonics in all types of stress measurement problems including the nondestructive measurement of residual stress.

The propagation velocity of ultrasonic waves in solids varies with stress in a manner that depends on the third-order elastic constants. In addition, shear wave velocity depends upon the angle between the polarization axis and the stress direction. These properties can combine to produce an effective rotation of the polarization axis as a shear wave travels through a stressed medium. Techniques for measuring these stress-dependent properties have been described in previous reports[1,2]* along with experimental results for several different materials.

The stress-dependent rotation of shear wave polarization is very similar to certain photoelastic effects. It also suffers many of the same limitations. One such limitation is that the total rotation observed is the integrated effect of travel through a given thickness. Thus, stress variations through a given thickness may produce a canceling effect and give results that are identical to those obtained in a stress-free medium. This problem has been solved in the case of photoelasticity through the development of a three-dimensional technique[3] which depends on certain peculiarities of scattering from a polarized light beam. A somewhat analogous technique is now theoretically possible using ultrasonic waves and the results described in this report.

II. STRESS-INDUCED BIREFRINGENCE

In the following sections of this report several areas of work are described relative to the use of ultrasonics in a technique of three-dimensional stress analysis. As a prelude to this study it was felt that additional information was needed about the behavior of shear waves in biaxially stressed samples. In earlier work we had limited our birefringence experiments to uniaxial stress conditions. Results of the earlier work[1,2]

Manuscript released by the authors February 1963 for publication as an ASD Technical Report.

*Numbers refer to references in Bibliography.

indicated that $\Delta V/V$ was linearly proportional to the uniaxial stress. An experiment was therefore set up to determine the relationship between $\Delta V/V$ and $P-Q$, the difference between the principal stresses in a biaxially stressed specimen.

The specimen shape and loading conditions are shown in Figure 1. The 8-in. diameter disk was 5/8 in. thick and made from 6061-T6 aluminum plate. Values of $\Delta V/V$ were determined at several different locations on the face of the plate using the pulse-echo technique described previously.[1] The compressive load was applied along a diameter of the disk either parallel or perpendicular to the rolling direction of the aluminum stock. The anisotropic rolling texture of aluminum produces a birefringence effect with principal axes parallel and perpendicular to the rolling direction. With the loading parallel to one of these principal axes, superposition of the original state (anisotropy due to preferred orientation) and the stress state produces a rotation of the resultant principal axes at all points on the face of the disk except along the two diameters that are parallel and perpendicular to loading. It was along these two (primary) diameters that measurements of $\Delta V/V$ were first made.

The value of $(P-Q)$ at any point (x,y) on the disk can be calculated using the expression[4]

$$P-Q = \frac{4rF(x^2+y^2-r^2)}{\pi\left[(x^2+y^2-r^2)^2 + 4r^2x^2\right]}$$

where r is the disk radius and F is the diametral load. The results of measurements at the center of the disk and one additional point on each of the two primary diameters conclusively showed that $\Delta V/V$ does vary linearly with $(P-Q)$.

In addition to measurements along the primary diameters, we made several attempts to verify the stress state at other points on the face of the disk. As mentioned before, the principal stress axes at these points rotate when the load is varied. Thus, the value of $(P-Q)$ as well as the directions of the principal axes varies from point to point and from one load to another. The fact that the axes at a given location rotate as the load is varied makes it necessary to rotate the transducer in order to evaluate $\Delta V/V$. Another problem arises because the transducers cover an area over which considerable variation may occur in both $(P-Q)$ and the principal axes' directions. These factors made it difficult to obtain clean pulse-echo patterns of the type used in accurate evaluations of $\Delta V/V$.

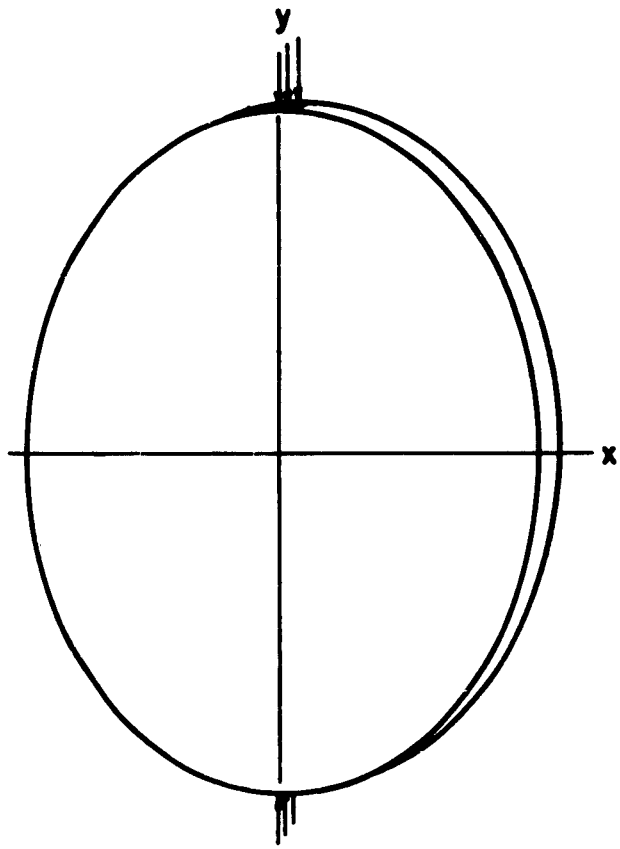

Figure 1 - Disk Loaded in Compression for Study of Biaxial Stress

III. GRAIN BOUNDARY SCATTERING FROM A SINGLE ULTRASONIC BEAM

The "scattering" technique[3] of three-dimensional photoelasticity has recently been refined to the point of being a very useful stress analysis tool. We will not go into the details of this technique, but a cornerstone of the whole procedure is the fact that polarized light waves produce maximum scattered radiation in directions perpendicular to the E-field vector, and minimum scattered intensity parallel to the E-field vector. It was felt that some of the techniques used in three-dimensional photoelasticity might be extended to the use of polarized shear waves and thus permit stress analysis in structural metals as well as transparent models. It was first necessary to study beam scattering in polycrystalline metals and determine if a spatial distribution exists similar to that exhibited by polarized electromagnetic radiation.

Our investigation of beam scattering has been limited to geometric arrangements similar to that shown in Figure 2. Initial experiments involved two 5-mc. AC-cut quartz crystals mounted on a block of aluminum as shown in Figure 2(a). The arrows on the transducers denote polarization direction. The small electrical signals produced by the receiver crystal were amplified and displayed on a CRT whose sweep was initiated when the transmitter was pulsed. With this arrangement we were able to determine the time delay between the transmitted pulse and receipt of the scattered signals. It was not surprising to find that a period of "quiet" followed the sweep initiation, but it was rather surprising to find that the first significant signals occurred at a time that corresponded to shear wave propagation along the path (d_1+d_2) as shown in Figure 2(b). This fact was verified at several values of d_1 and d_2. A few very weak signals are sometimes present between t_o and $t_{(d_1+d_2)}$ but they are usually much weaker than those occurring at $t_{(d_1+d_2)}$. We believe the earlier signals come from beam spreading, mode conversion, and multiple scattering which may permit a more direct path of travel between the two transducers.

The magnitude of the first strong signal is very sensitive to slight translations of either the transmitter or receiver crystals. This is probably due to variations in the grain structure that produces the scattering. The lack of reproducibility in the received signal amplitude made it impossible to observe any systematic variation in scattered intensity as the polarization direction of either crystal was varied. Thus, we have been unable to definitely pinpoint a spatial variation in the energy scattered from a polarized shear wave.

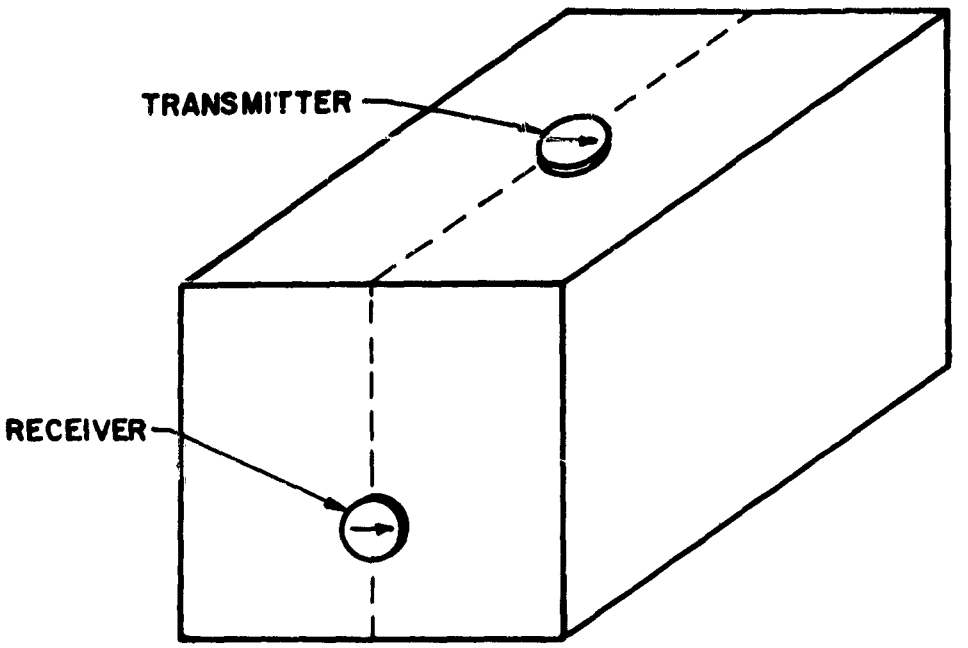

(a)

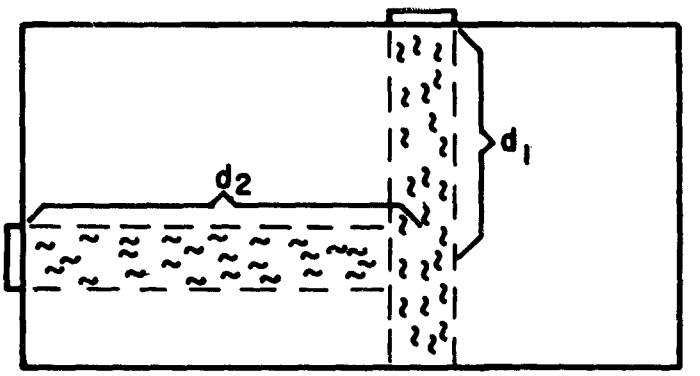

(b)

Figure 2 - Schematic Diagrams of (a) Test Block With Transducers, and (b) Section Showing Apparent Path of Primary Wave and Scattered Signal

The study of beam scattering was next extended to include various combinations of X-cut and AC-cut transmitter and receiver crystals. In each case, the resonant frequency of both crystals was the same. The magnitude of the received signal was much greater when AC-cut crystals were used for both transmitter and receiver than any other combination of AC-cut and X-cut crystals.

In the previous discussions we have been interested only in the intensity of the first signals to reach the receiver crystal. Subsequent signals are numerous and ultimately run together to form an almost continuous "noise" along the CRT sweep. Multiple reflections, beam spreading, and mode conversions give rise to this relatively high intensity noise which finally dies out as the energy of the primary wave is dissipated.

IV. INTERACTION OF TWO ULTRASONIC WAVES

A. General Theory

The details of the theoretical analysis of elastic wave interaction in nonlinear solids were given in a previous report[2] and therefore will not be repeated here. Let it suffice to say that an interaction between two waves is predicted and a "scattered" wave of combination (sum or difference) frequency theoretically originates at the region of intersection. The intensity of the scattered wave is expected to be a maximum when so-called resonant conditions exist. Table 1 summarizes the various types of interaction predicted by theory and gives expressions for $(\cos \varphi)$ where φ is the angle between the primary beams at resonance.

In reference 2, it was pointed out that from a quantum mechanical standpoint the phonon-phonon interaction should give rise only to phonons with the sum of the frequencies of the primary phonons due to conservation of wave vector $(\vec{k}_3 = \vec{k}_1+\vec{k}_2)$ and energy $(\omega_3 = \omega_1+\omega_2)$. It will be shown in the following discussion that the classical treatment which predicts a scattered wave with the difference frequency $(\omega_1-\omega_2)$ also has its quantum mechanical analogy. The argument is based on a paper by Slonimskii[5] on sound absorption in solids.

It seems obvious that, if it is possible for two phonons to combine to give a third one of frequency $\omega_3 = \omega_1+\omega_2$, the reverse process can occur as well, i.e., one phonon of frequency ω_3 may split into two under the condition: $\omega_3 = \omega_1 + (\omega_3-\omega_1)$. If $(\omega_3-\omega_1)$ is set equal to ω_2, the

TABLE 1

INTERACTION CASES WHICH PRODUCE A SCATTERED WAVE

Case	Primary Waves	Resonant Wave Type and Frequency	Direction of Scattered Wave	cos φ *
I	Two transverse	Longitudinal $(\omega_1+\omega_2)$	$\vec{k}_1+\vec{k}_2$	$c^2+\left[(c^2-1)(a^2+1)\,/\,2a\right]$
II	Two longitudinal	Transverse $(\omega_1-\omega_2)$	$\vec{k}_1-\vec{k}_2$	$1/c^2+\left[(c^2-1)(a^2+1)\,/\,2ac^2\right]$
III	One longitudinal and one transverse**	Longitudinal $(\omega_1+\omega_2)$	$\vec{k}_1+\vec{k}_2$	$c+\left[a(c^2-1)\,/\,2c\right]$
IV	One longitudinal and one transverse**	Longitudinal $(\omega_1-\omega_2)$	$\vec{k}_1-\vec{k}_2$	$c+\left[a(1-c^2)\,/\,2c\right]$
V	One longitudinal and one transverse**	Transverse $(\omega_1-\omega_2)$	$\vec{k}_1-\vec{k}_2$	$1/c+\left[(c^2-1)\,/\,2ac\right]$

* φ is the angle between $\vec{k}_1$ and $\vec{k}_2$ at resonance.
a is the frequency ratio ω_2/ω_1.
c is the velocity ratio C_t/C_ℓ.
**The frequency of the longitudinal primary wave is ω_1.

equivalence of the two relations is clear. If the wavelengths of the phonons involved are sufficiently greater than the lattice spacing so that dispersion and Umklapp processes need not be considered, it is easily seen from the conservation laws that only longitudinal phonons may split into two phonons. The resultant phonons may both be transverse or one may be longitudinal and the other transverse.

The elastic waves are represented as a sum of harmonic waves

$$\vec{U}(\vec{r}) = \sum_{\alpha} \vec{u}_{\alpha}(\vec{k}_{\alpha},\vec{r})$$

$$\text{with } \vec{u}_{\alpha}(\vec{k}_{\alpha},\vec{r}) = \vec{e}_{\alpha}(a_{\alpha}e^{i\vec{k}_{\alpha}\cdot\vec{r}} + a_{\alpha}^{*}e^{-i\vec{k}_{\alpha}\cdot\vec{r}}) \tag{1}$$

where $\vec{e}_{\alpha}$ is a unit vector in the direction of polarization, a_{α} is the amplitude, and $\vec{k}_{\alpha}$ the propagation vector. If N_{α} represents the number of phonons in a particular mode α, the matrix elements of the displacement operator, according to the theory of the harmonic oscillator, are:

$$\langle N_{\alpha}-1|a_{\alpha}|N_{\alpha}\rangle = \left(\frac{\hbar N_{\alpha}}{2m\omega_{\alpha}}\right)^{\frac{1}{2}} e^{-i\omega_{\alpha}t}$$

$$, \tag{2}$$

$$\langle N_{\alpha}|a_{\alpha}^{*}|N_{\alpha}-1\rangle = \left(\frac{\hbar N_{\alpha}}{2m\omega_{\alpha}}\right)^{\frac{1}{2}} e^{i\omega_{\alpha}t}$$

where m is the mass of the volume of interest. We are interested in the transition probability from a state with number of phonons N_1, N_2, N_3 to a state with number of phonons N_1-1, N_2+1, N_3+1. The part of the elastic energy expansion containing cubic strain terms is taken as the perturbing Hamiltonian H_p. It is shown[5] that H_p can be evaluated to give:

$$H_p^{(1)} = i\left[2B(a+b)+2Ac\right]\vec{u}^{(1)}\left[\vec{k}_1,\vec{r}\right]\vec{u}^{(2)}\left[\vec{k}_2,\vec{r}\right]\vec{u}^{(3)}\left[\vec{k}_3,\vec{r}\right] \tag{3}$$

for the decay of a longitudinal phonon into one longitudinal and one transverse phonon, and

$$H_p^{(2)} = i\left[2Bb+2Ac+(K-2/3\mu)d-2\mu f\right]\vec{u}^{(1)}\left[\vec{k}_1,\vec{r}\right]\vec{u}^{(2)}\left[\vec{k}_2,\vec{r}\right]\vec{u}^{(3)}\left[\vec{k}_3,\vec{r}\right] \qquad (4)$$

for the decay of a longitudinal phonon into two transverse phonons. A and B are third-order elastic constants and a , b , c , d , f are expressions containing the wave vectors and polarizations, i.e., $a = (\vec{k}_1,\vec{k}_2,\vec{k}_3,\vec{e}_1,\vec{e}_2,\vec{e}_3)$. The matrix elements are then

$$\langle N_1,N_2,N_3\left|H_p^{(1)}\right|N_1-1,N_2+1,N_3+1\rangle$$
$$= i\left[2B(a+b)+2Ac\right]\left(\frac{\hbar N_1}{2m\omega_1}\right)^{\frac{1}{2}}\left(\frac{\hbar(N_2+1)}{2m\omega_2}\right)^{\frac{1}{2}}\left(\frac{\hbar(N_3+1)}{2m\omega_3}\right)^{\frac{1}{2}} e^{-i\left[\vec{K}\cdot\vec{r}-\Omega t\right]} \qquad (5)$$

for the case (3) where $\vec{K} = \vec{k}_1-\vec{k}_2-\vec{k}_3$, and $\Omega = \omega_1-\omega_2-\omega_3$. Integrating over the volume V and calculating the transition probability per unit time according to perturbation theory one obtains:

$$W^{(1)} = \frac{2\pi\hbar}{(2m)^3}\frac{N_1(N_2+1)(N_3+1)}{\omega_1\omega_2\omega_3}\left[2B(a+b)+2Ac\right]^2\delta(\Omega)\left[\int_V e^{-i\vec{K}\cdot\vec{r}}\,d^3r\right]^2 \qquad (6)$$

The volume integral goes rapidly to zero for $K \neq 0$ if V is large compared to the wavelengths involved. When $K = 0$, we see that $W^{(1)}$ is proportional to V^2 . Using expression (4) a similar expression is obtained for the transition probability of a longitudinal phonon into two transverse phonons.

It is now apparent how the generation of an elastic wave of frequency $(\omega_1-\omega_2)$, as predicted classically, can also be predicted from a quantum mechanical standpoint. Furthermore, the quantum mechanical treatment allows an easy calculation of the intensities. Equation (6) shows that the transition probability is proportional to the number of phonons involved in the process. Now, consider the state $|N_1,N_2,N_3\rangle$, from which the transition to the state $|N_1-1,N_2+1,N_3+1\rangle$ will be made. Note that the transition probability is enhanced by a large N_2 just as it is by a large N_1 . In other words, if two elastic waves with frequencies $(\omega_1 > \omega_2)$ intersect under the right conditions as outlined above, the interaction results in a reduction of the intensity of the wave ω_1 . The amount is partly added to

the intensity of the wave ω_2 and partly gives rise to a third wave of frequency $(\omega_1-\omega_2)$. One might say that the second wave stimulates the splitting of the phonons of the first wave. This "maser"-like interaction may have some further significance.

The correspondence between the classical and quantum mechanical treatment of two interacting elastic waves in a solid now appears more reasonable. Both treatments lead to the same conditions for the angle of intersection of the two waves to produce a third one of either the sum or difference frequency, and also give the right polarizations of the three waves relative to each other. It is expected further that, for the same intensities of the two primary waves, the intensity of a scattered wave with frequency $(\omega_1-\omega_2)$ is less than the intensity of a scattered wave with frequency $(\omega_1+\omega_2)$, since in the latter case two phonons combine to give a third one corresponding to the transition from a state $|N_1,N_2,N_3\rangle$ to a state $|N_1-1,N_2-1,N_3+1\rangle$.

B. Intensity of Interaction

Using the techniques described in a previous report, expressions have been derived for the amplitude of scattered waves from all of the possible interaction cases. These expressions are given in Appendix A. The most favorable conditions for detecting beam interaction should occur when the amplitude of the scattered wave is maximum. Obviously the maximum should occur under conditions of resonance, but it should be remembered that resonance can occur over a finite range of (a) values. The amplitude expressions shown in Appendix A were therefore programmed for an IBM 1620 computer and numerical results were obtained for various values of the frequency ratio, (a), and for most of the materials for which third-order elastic constants are available.[6,7]

Figures 3 - 9 are plots of amplitude factors for four different materials in each of the seven cases that yields a nonzero amplitude expression. The amplitude is directly proportional to the factor γ through the expression

$$\text{amplitude} = \left(\frac{X_1 X_2 f_1^3 V}{R}\right)\gamma \qquad (7)$$

where X_1 and X_2 are the amplitudes of the primary waves, f_1 is the frequency in mc/sec, V is the volume of intersection, and R is the distance between the "point" of intersection and the point of observation.

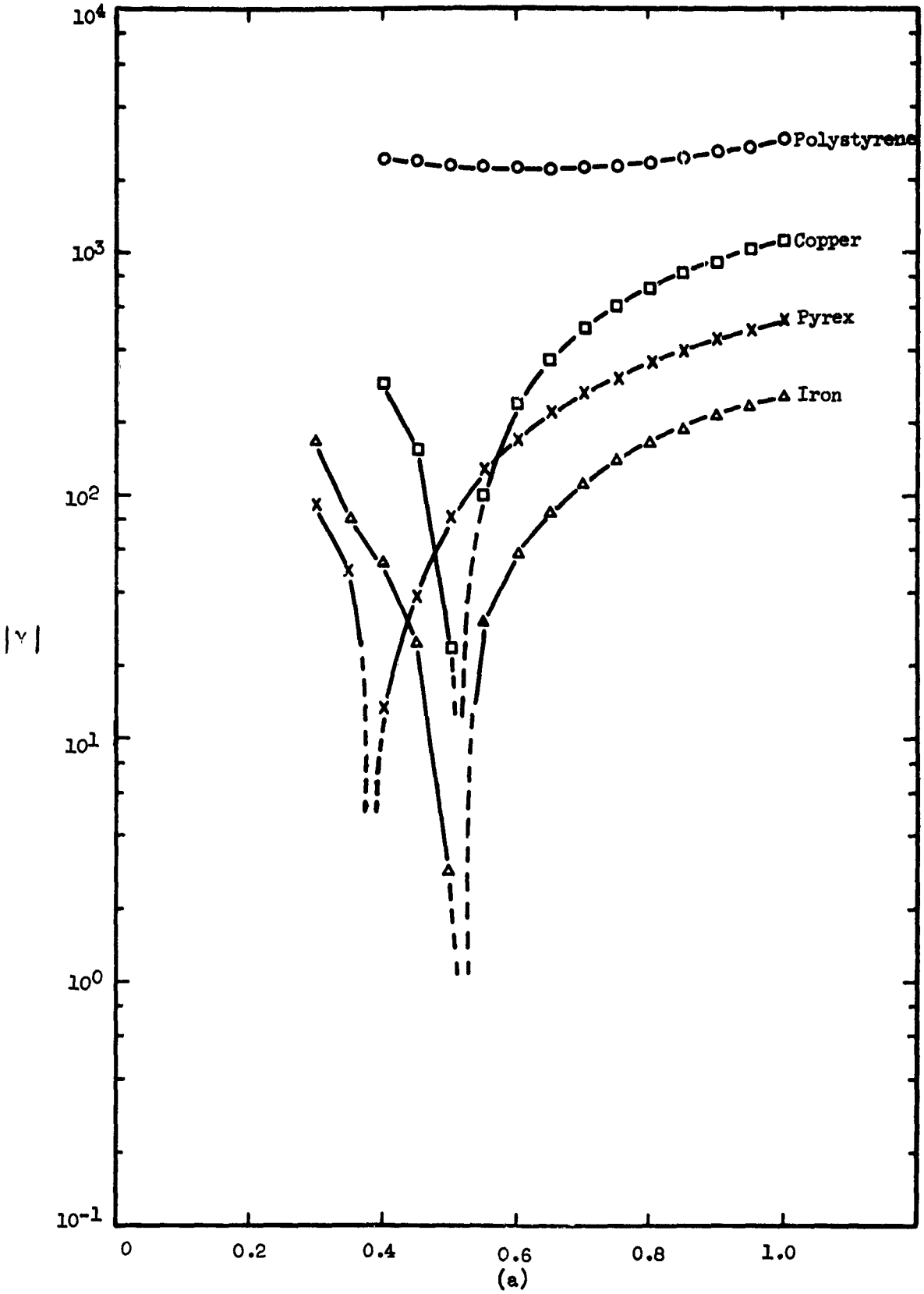

Figure 3 - Amplitude Factors for the Interaction of Two Transverse Waves to Produce a Scattered Longitudinal Wave (Case I-A). Both Primary Waves Polarized Perpendicular to $\bar{K}_1\bar{K}_2$ Plane.

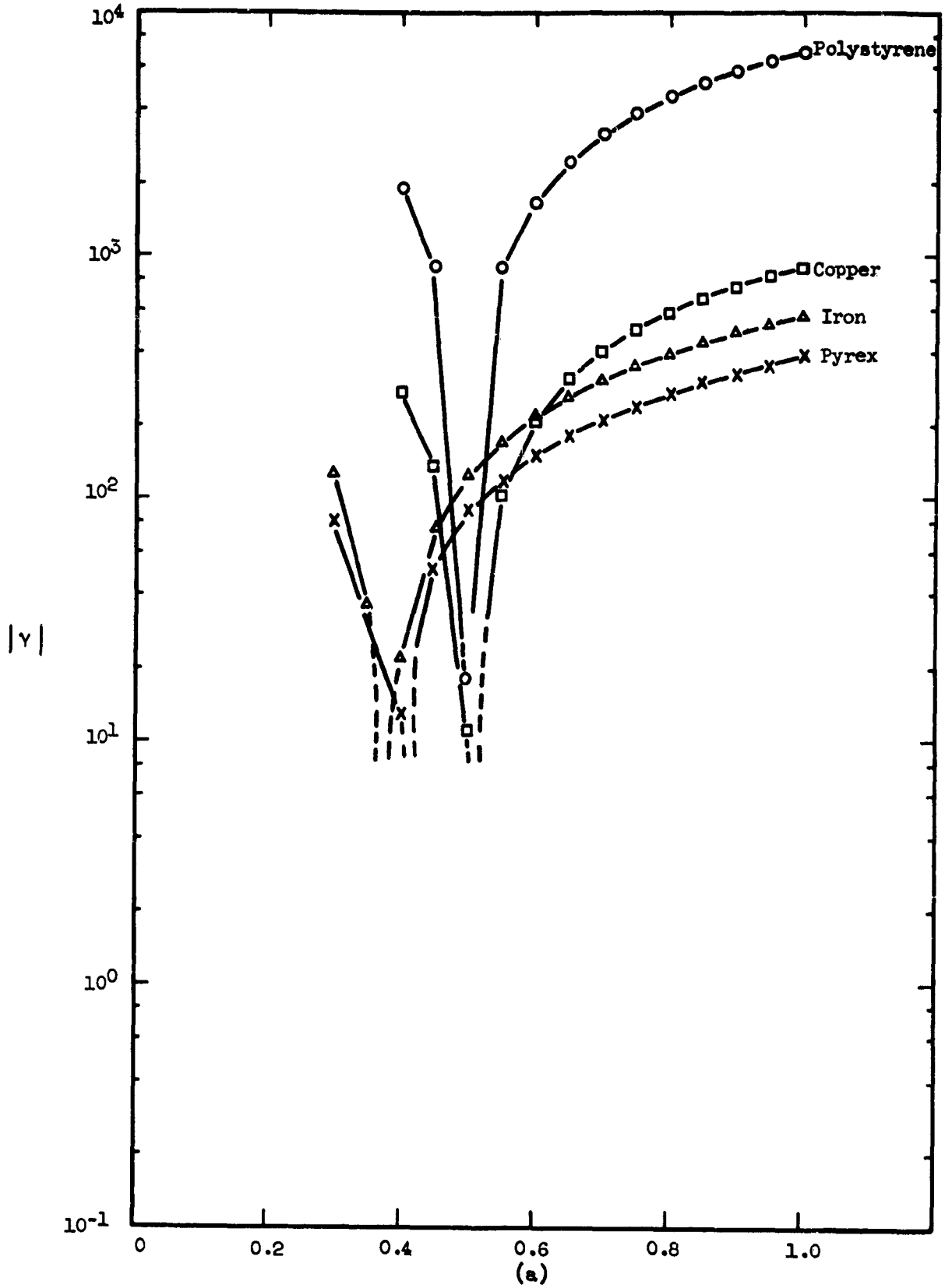

Figure 4 - Amplitude Factors for the Interaction of Two Transverse Waves to Produce a Scattered Longitudinal Wave (Case I-B). Both Primary Waves Polarized Parallel to $\bar{k}_1\bar{k}_2$ Plane.

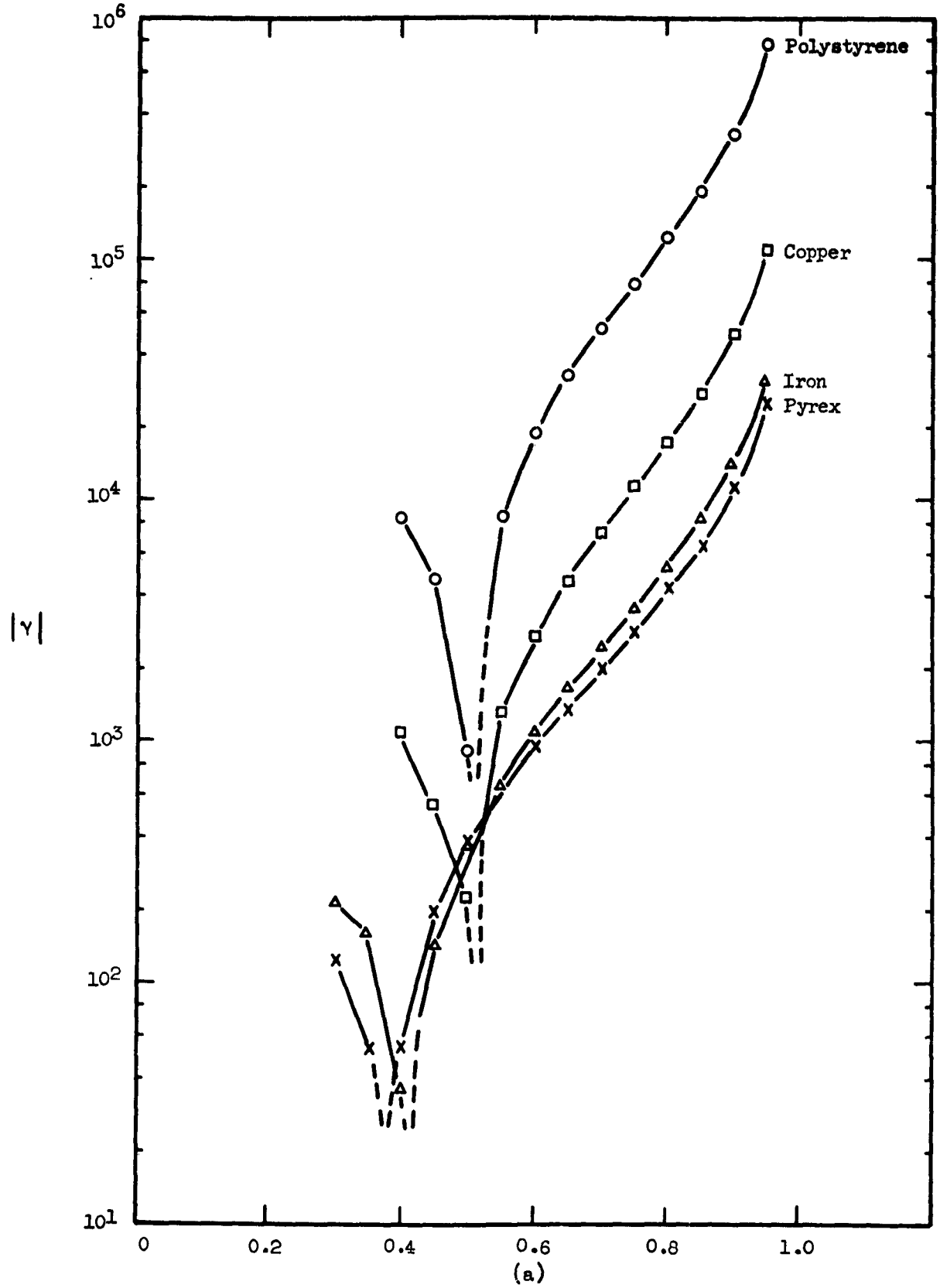

Figure 5 - Amplitude Factors for the Interaction of Two Longitudinal Waves to Produce a Scattered Transverse Wave (Case II)

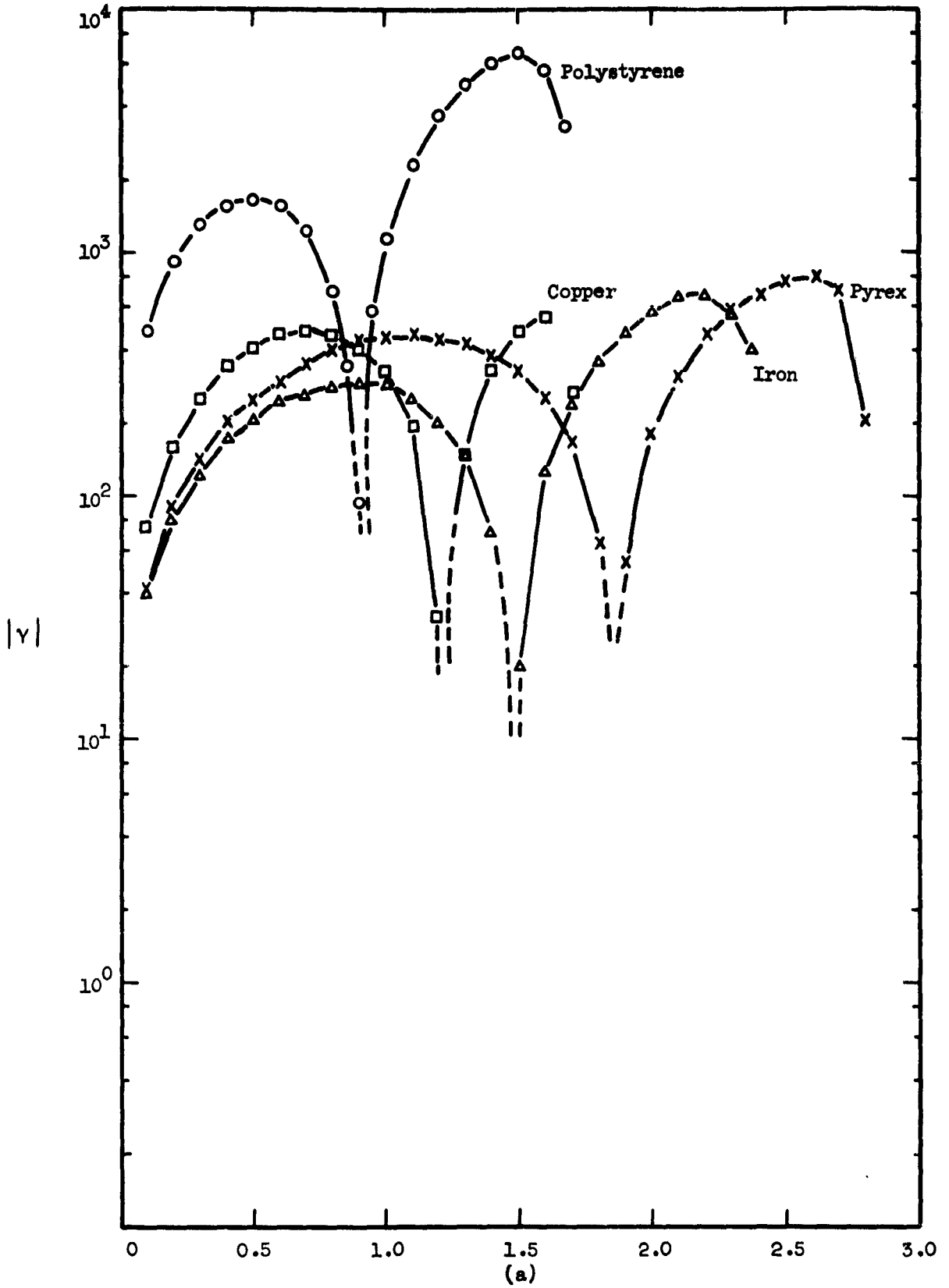

Figure 6 - Amplitude Factors for the Interaction of a Longitudinal and a Transverse Wave to Produce a Summed Frequency Longitudinal Wave (Case III-A). The Primary Transverse Wave is Polarized Parallel to the $\bar{k}_1\bar{k}_2$ Plane.

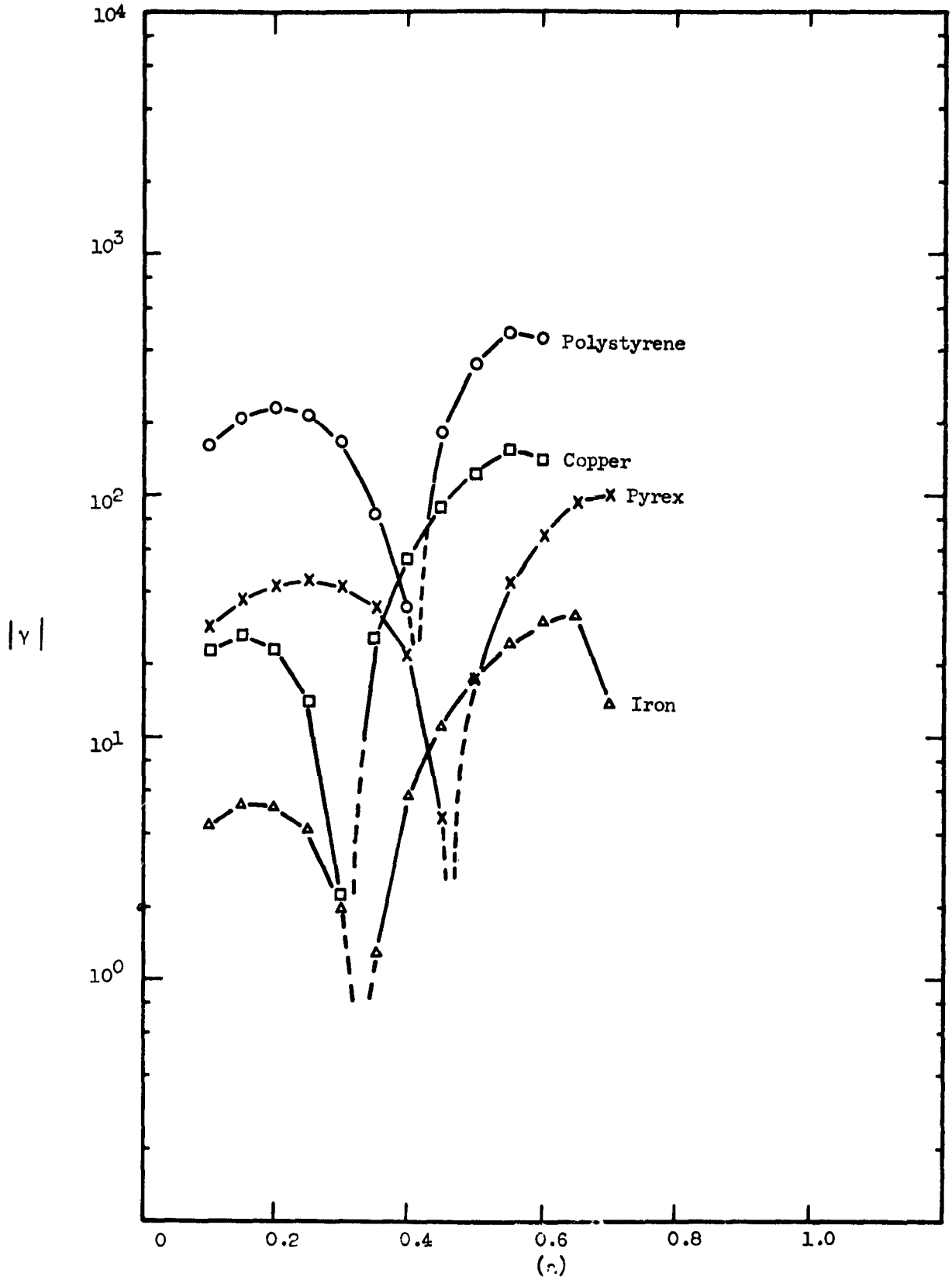

Figure 7 - Amplitude Factors for the Interaction of a Longitudinal and a Transverse Wave to Produce a Difference Frequency Longitudinal Wave (Case IV-A). The Primary Transverse Wave is Polarized Parallel to the $\bar{k}_1\bar{k}_2$ Plane.

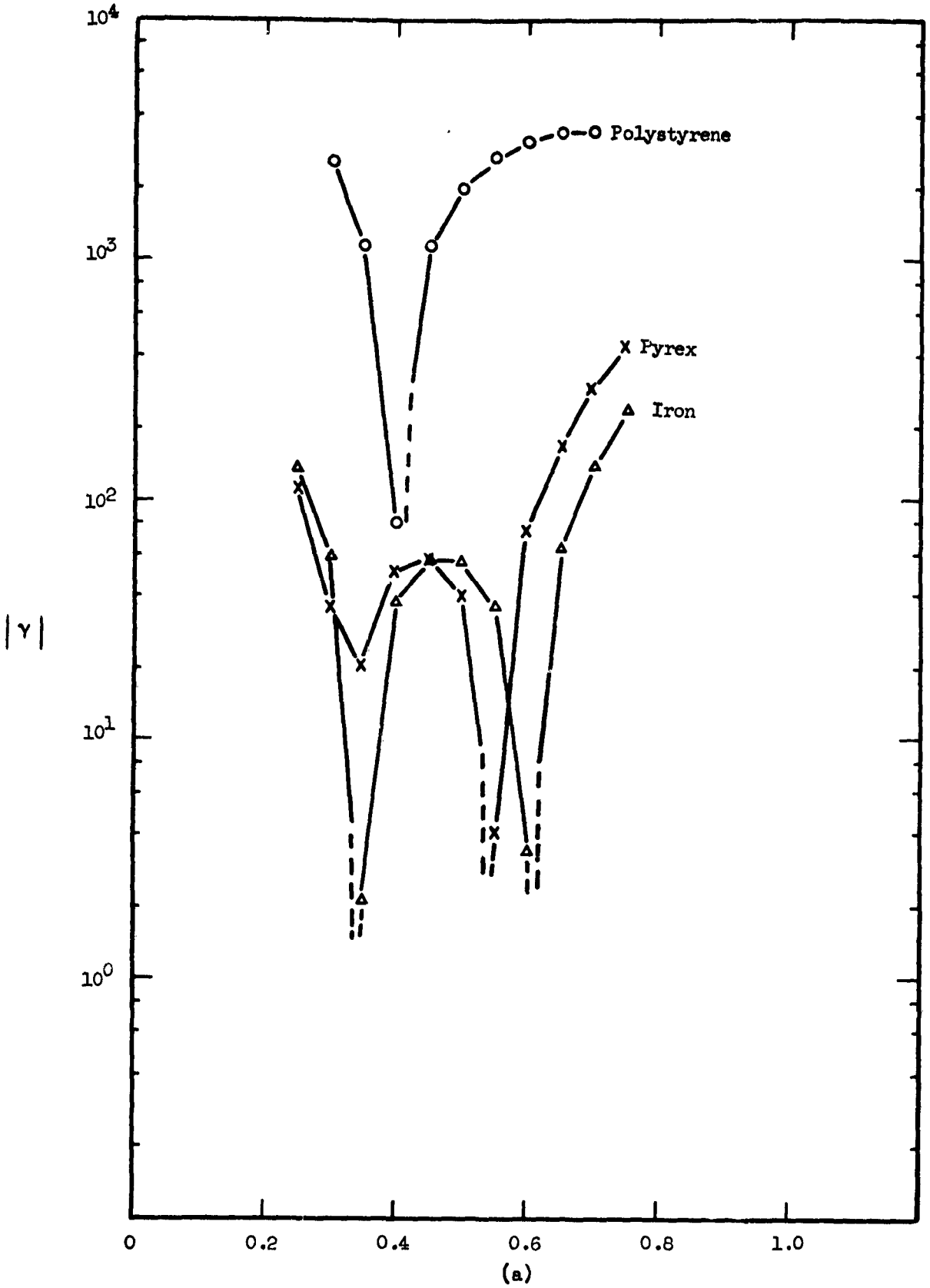

Figure 8 - Amplitude Factors for the Interaction of a Longitudinal and a Transverse Wave to Produce a Difference Frequency Transverse Wave (Case V-A). The Primary Transverse Wave is Polarized Perpendicular to the $\bar{k}_1\bar{k}_2$ Plane.

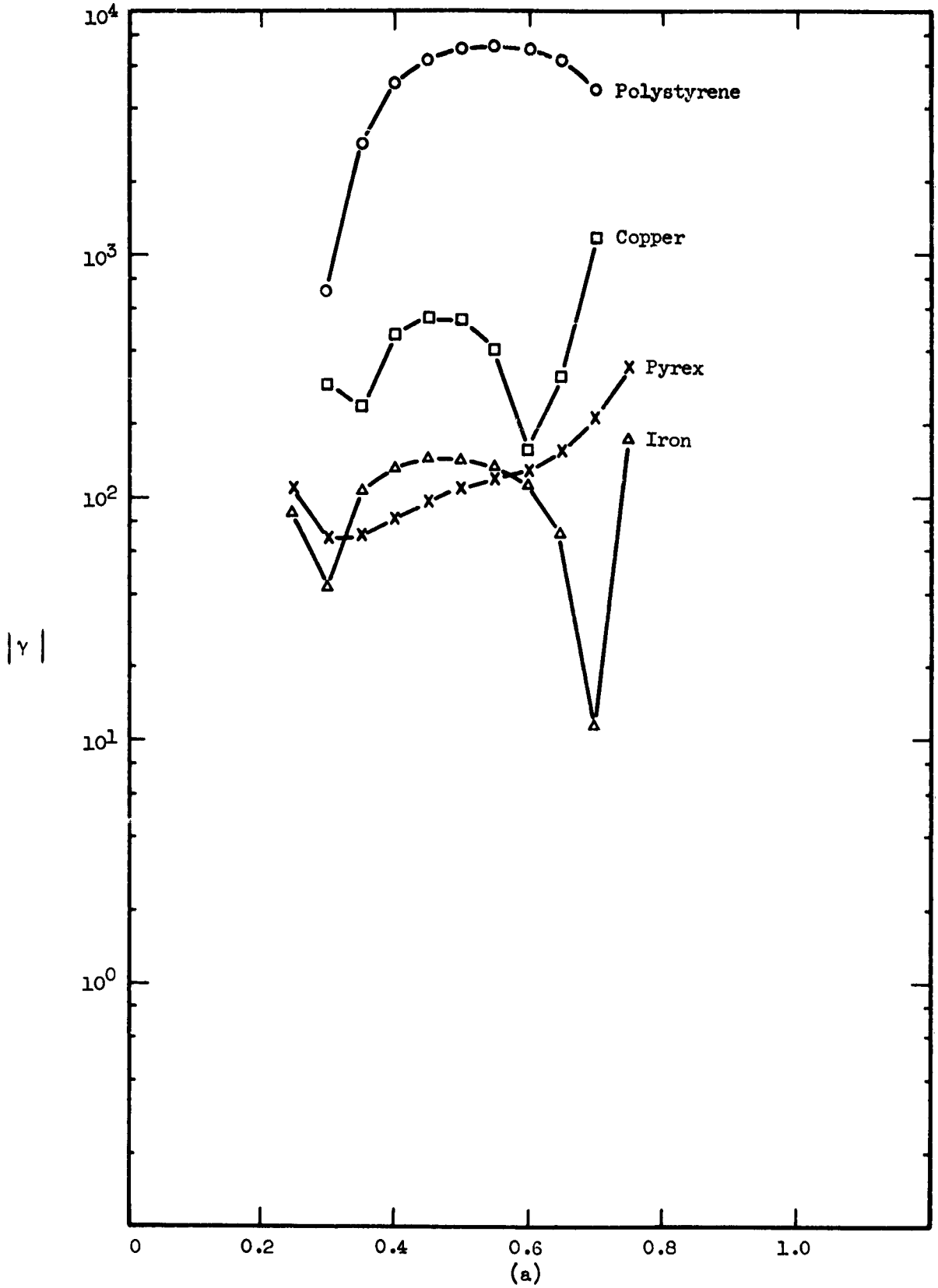

Figure 9 - Amplitude Factors for the Interaction of a Longitudinal and a Transverse Wave to Produce a Difference Frequency Transverse Wave (Case V-B). The Primary Transverse Wave is Polarized Parallel to the $\bar{k}_1\bar{k}_2$ Plane.

γ has the dimensions of sec^3/cm^3 in the c.g.s. system used here. We see that γ is free of all of the experimental variables except the frequency ratio (a) and the physical constants of the material under investigation. It has been mentioned previously[2] that the amplitude expressions were derived for the following conditions:

$$R \gg V^{1/3} \gg \lambda_s$$

where λ_s is the wavelength of the scattered wave. These conditions, of course, prohibit R from going to zero in (7) above.

In Figures 3 - 9, we have plotted the absolute values of γ. The real value of γ may be negative as well as positive, but the intensity of the scattered wave is proportional to γ^2 and therefore always positive. In plotting the data we have used dashed lines near those areas where the real value of γ changes sign. The absolute value of γ always shows a minimum near such areas as it actually goes to zero. The exact locations of these zero intensity points have not been accurately determined because we are more interested in the intensity maxima.

The information contained in the (γ versus a) plots can be used in optimizing the experimental variables. The curves are particularly helpful in locating relatively sharp maxima such as those shown in Figure 6. In general, we see that the intensity of the interaction should be larger in polystyrene than any of the other materials examined here. One might have guessed this on intuitive grounds and we expect that other "plastics" would probably compare favorably with polystyrene. It should be remembered, however, that the calculations consider all materials as dissipationless. Expression (7) indicates the scattered amplitude has a very strong dependence on frequency as well as amplitude of the primary waves. It is possible (and indeed probable) that a material with a high γ will be particularly absorptive and therefore attenuate both the primary and scattered waves much more rapidly than materials with a low γ.

C. Experimental Details and Results

Figure 10 shows a block diagram of a typical setup for observation of scattered waves produced by ultrasonic beam interaction. The triangular specimen is cut so that the intersection angle φ satisfies the resonant condition for interaction. Transducers (A) and (B) are driven by separate rf pulse generators and produce the two primary waves. An Arenberg pulsed oscillator model PG-650C is used to drive one transducer and the pulsed oscillator

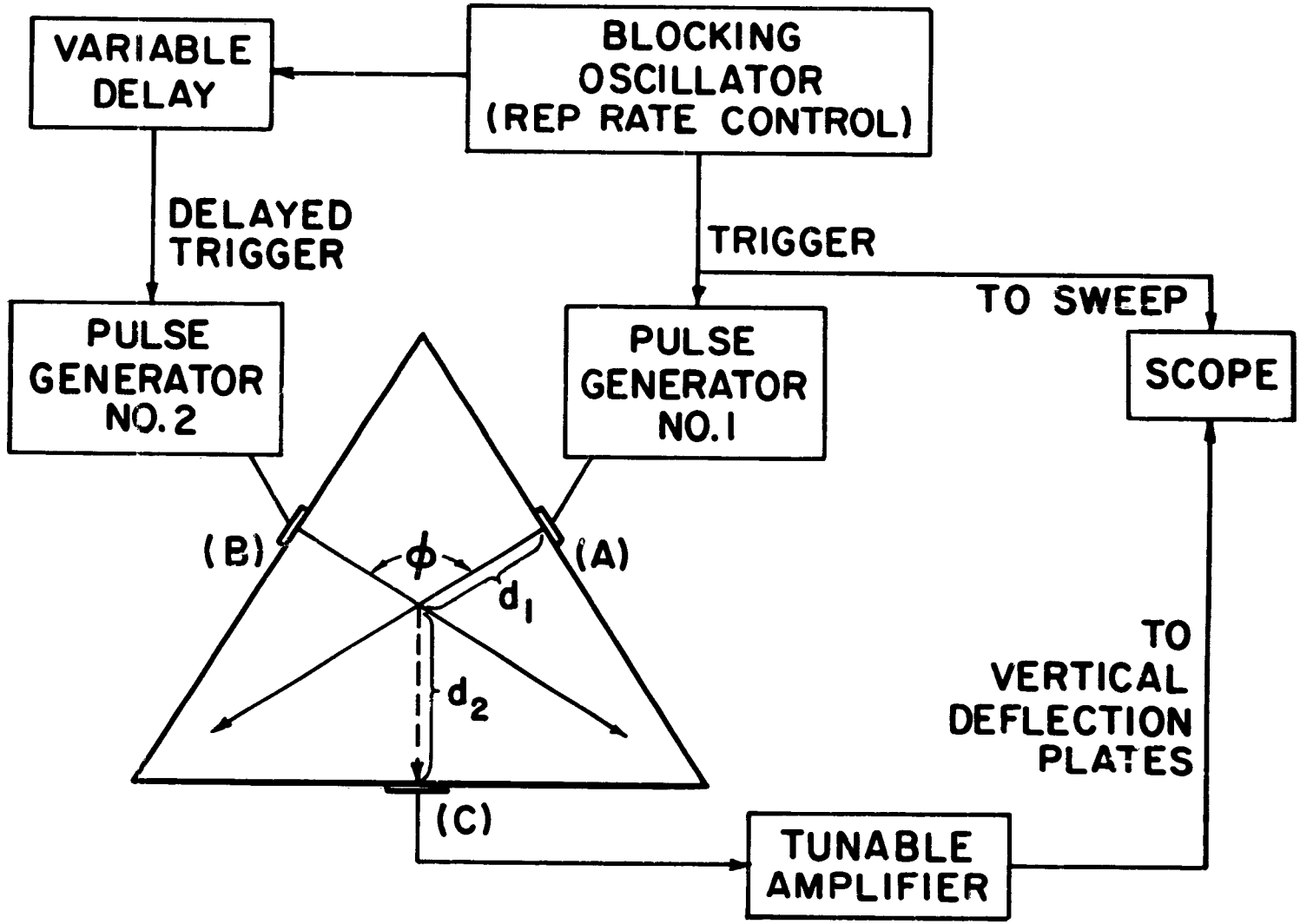

Figure 10 - Block Diagram of Test Piece and Associated Electronics

portion of a Sperry ultrasonic attenuation comparator is used to drive the second transducer. Transducer (C) is used as a receiver for the scattered wave. At time t_o a signal from the blocking oscillator triggers Pulse Generator No. 1 and the oscilloscope sweep. A variable delay is used to trigger Pulse Generator No. 2 at (t_o+t_d) where t_d is the delay. The tunable amplifier has a bandwidth of approximately 1.5 mc/sec at the 3 db points, and operating into the scope it produces a maximum deflection of approximately 5 mv/in at 5 mc/sec. Quartz transducers have been used exclusively; therefore, impedance matching circuits have been used between the transducers and the generators or amplifier.

Isolation and identification of the scattered signals are accomplished in a number of ways. First, the time of arrival of the scattered signal at transducer (C) should correspond to acoustic propagation along paths d_1 and d_2. It should be recalled that the velocity of propagation along leg d_1 may be different than that along d_2. For example, the triangular specimen illustrated in Figure 1 was made up for the interaction of two transverse waves of frequencies ω_1 and ω_2 to produce a longitudinal wave of frequency $\omega_3 = \omega_1+\omega_2$. Thus, the scattered signal should arrive at (C) at time $(t_o+d_1/c_t+d_2/c_\ell)$. The time can easily be determined with the calibrated sweep of the oscilloscope. Transducer (C) is, of course, selected by frequency and mode to match the expected scattered wave. Amplifier tuning reveals the frequency of the detected signal. In addition, the setting of t_d must be selected so that both primary wave packets pass through the volume of interaction at approximately the same time.

Figure 11 is an oscillogram showing a typical scattered wave pulse (indicated by arrow) and illustrates the signal to noise relationship. The signal amplitude will drop severely if (1) the amplitude of either primary wave is reduced, (2) the frequency of either primary wave is changed, (3) the amplifier is tuned off the expected ω_3 frequency, or (4) t_d is varied from the calculated value.

During the past few months we have experimentally confirmed each of the five theoretical interaction cases enumerated in Table 1. The successful detection of a "scattered" beam was first attained in a triangular specimen of fused silica using Case I, i.e., interaction of two transverse waves to produce a sum frequency longitudinal wave. For short-hand purposes let us refer to such an interaction as follows: $T(\omega_1)+T(\omega_2) = L(\omega_1+\omega_2)$. The actual case studied in the fused silica specimen was $T(5)+T(5) = L(10)$. Theory predicts (as shown in Appendix A) that a scattered wave should be generated when the two transverse waves are both polarized in the $(\bar{k}_1,\bar{k}_2)$ plane or when both are polarized perpendicular to the $(\bar{k}_1,\bar{k}_2)$ plane. It further predicts that the signal amplitude should be zero when one primary wave is polarized in the $(\bar{k}_1,\bar{k}_2)$ plane and the other is polarized perpendicular to the plane.

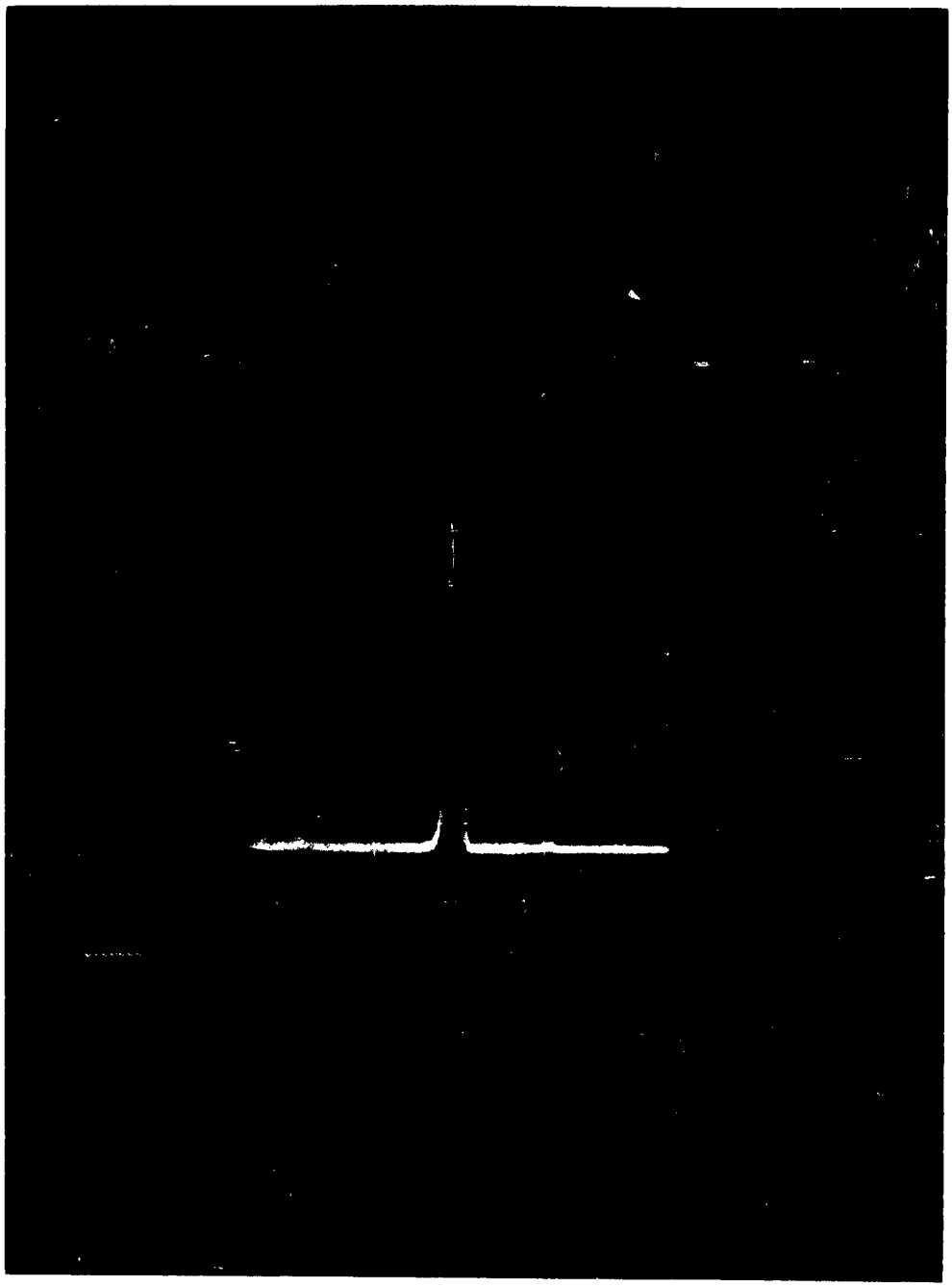

Figure 11 - Oscillogram Showing Signal Produced by Scattered Wave

We have experimentally confirmed all these predictions using the fused silica specimen. Using the same specimen we have replaced the two 5-mc/sec crystals with one 3- and one 7-mc/sec crystal. Although the sum frequency is still 10 mc/sec we have been unable to detect a scattered signal. These negative results agree with theory, of course, because the specimen was not cut to produce resonant interaction between beams of 3 and 7 mc/sec.

We have also performed several experiments to determine the degree of collimation exhibited by the scattered wave. One such experiment is illustrated in Figure 12. With the primary transducers arranged symmetrically as shown in Figure 12a, the maximum scattered signal was detected with the receiving transducer centered at position O . When the receiving transducer was moved 1 cm. either way to position X or Y , the amplitude of the scattered signal fell to less than one-tenth the value obtained at O . If the primary transducers are rearranged as in Figure 12b (and t_d is adjusted to the appropriate delay) we now find the maximum scattered signal at position O' .

The interaction case, L(5)+T(5) = L(10) , was studied in a specimen of 6061-T6 aluminum similar to that illustrated in Figure 13. A 10-mc/sec longitudinal wave was detected approximately 18 μsec after t_o . The calculated travel time along d_1 and d_3 is shown to be 17.8 μsec. Furthermore, the scattered signal was observed only when the delay time t_d was approximately 3 μsec. This agrees well with the calculated delay of 3.5 μsec. In the above case, it was found that the magnitude of the scattered signal was maximum when the polarization of the transverse wave was in the $(\bar{k}_1, \bar{k}_2)$ plane and zero when rotated to the perpendicular position. This result also agrees with theory (see Appendix A).

In the experiments just described the two primary waves were always the same frequency. This leads to the production of a sum frequency equal to $2\omega_o$, a rather unfortunate case since the second harmonic of the primary frequency is involved. In subsequent experiments different primary frequencies were often used. Many of these experiments have been performed on magnesium due to the relatively large interaction effects exhibited by that material. The following cases have all been investigated in magnesium.

$$T(5)+T(5) = L(10)$$

$$L(10)+T(5) = T(5)$$

$$L(7)+T(3) = L(10)$$

$$L(10)+T(3) = L(7)$$

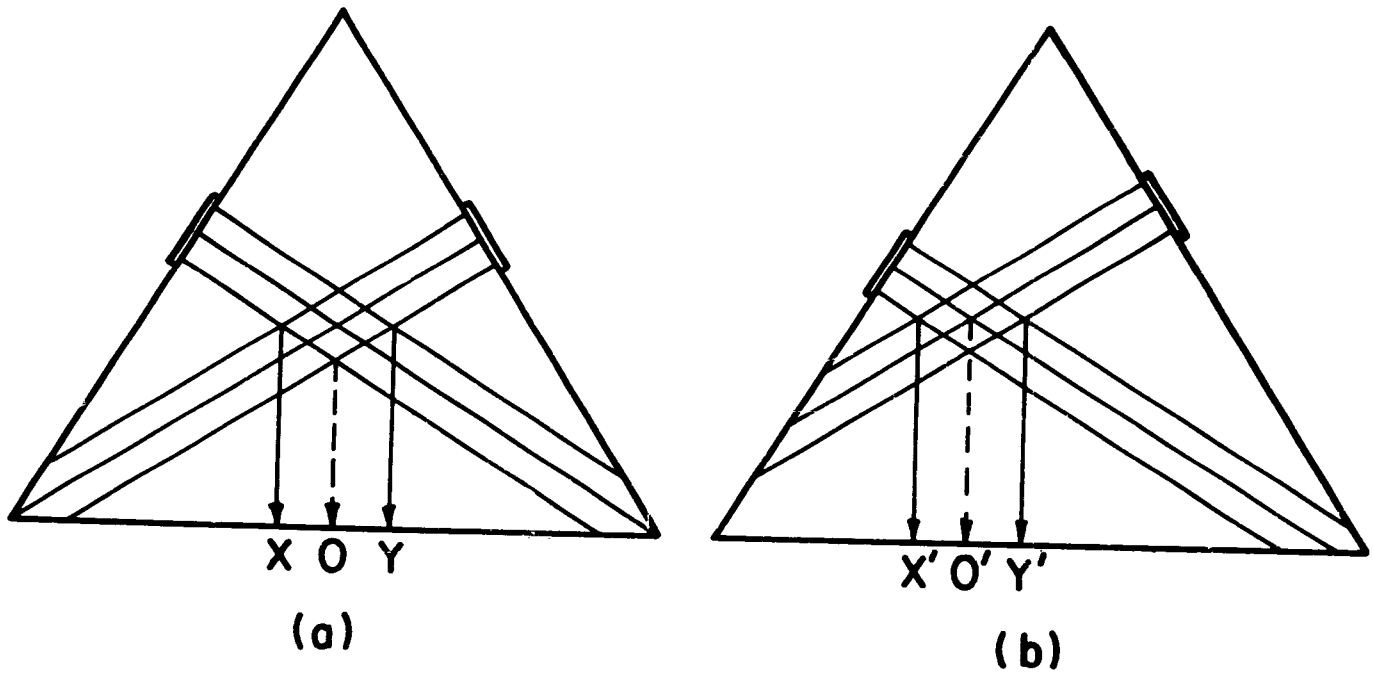

Figure 12 - Diagram Showing Location of Scattered Signal for Different Transducer Arrangements

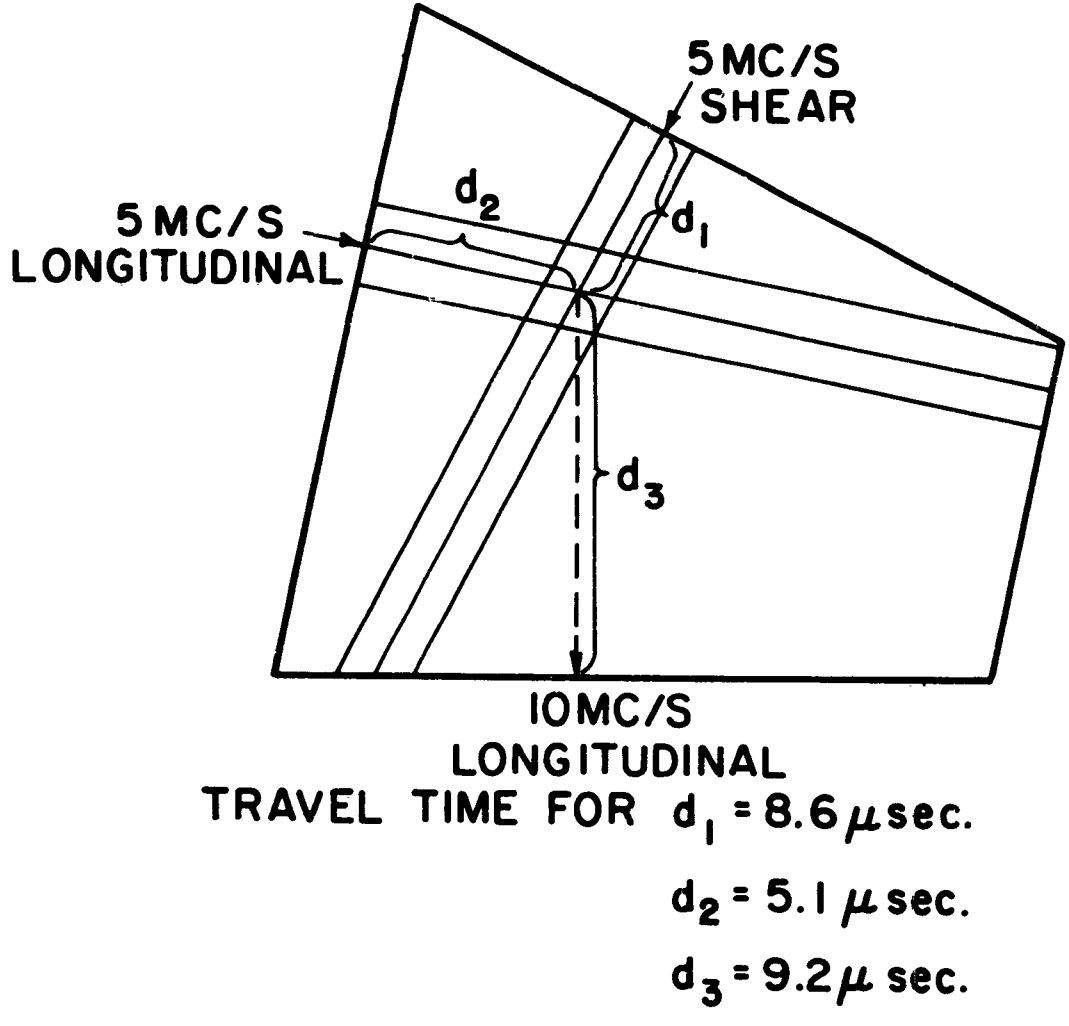

Figure 13 - Interaction of Longitudinal and Shear Waves in Specimen of Polycrystalline 6061-T6 Aluminum Alloy

$$L(15)+L(10) = T(5)$$

$$L(15)+T(5) = L(10)$$

$$L(10)+T(5) = L(15)$$

$$L(5)+T(3) = L(8)$$

$$L(5)+L(8) = T(3)$$

$$L(8)+T(3) = L(5)$$

Most of the above cases were studied using disk-like specimens similar to that shown in Figure 14. Small flats are machined at selected points on the disk circumference to permit the application of transducers. The flats are perpendicular to the disk radii; thus, interaction between the primary beams always occurs at the center of the disk. If each flat has a parallel flat on the opposite side of the disk, as represented by positions A' , B' and C' , then several interaction cases can be studied. For example, consider a 5-mc. longitudinal wave, $\bar{k}_1$, intersecting a 3-mc. shear wave, $\bar{k}_2$, to produce an 8-mc. longitudinal wave, $\bar{k}_3$. The angle φ_1 must satisfy the resonant condition for this interaction and the scattered wave travels in the $\bar{k}_3$ direction as defined by $(\bar{k}_1+\bar{k}_2)$. By close examination it becomes obvious that all of the interaction cases listed in Table 2 can be studied.

TABLE 2

INTERACTION CASES THAT CAN BE STUDIED
ON SPECIMEN SHOWN IN FIGURE 14

Interaction Case	Resonance Angle	Direction of Primary Waves	Direction of Scattered Wave
$L(5)+T(3) = L(8)$	φ_1	$\bar{k}_1$ and $\bar{k}_2$	$\bar{k}_3$
$L(8)+T(3) = L(5)$	φ_2	$\bar{k}_3$ and $\bar{k}_2$	$\bar{k}_1$
$L(8)+L(5) = T(3)$	φ_3	$\bar{k}_3$ and $\bar{k}_1$	$\bar{k}_2$

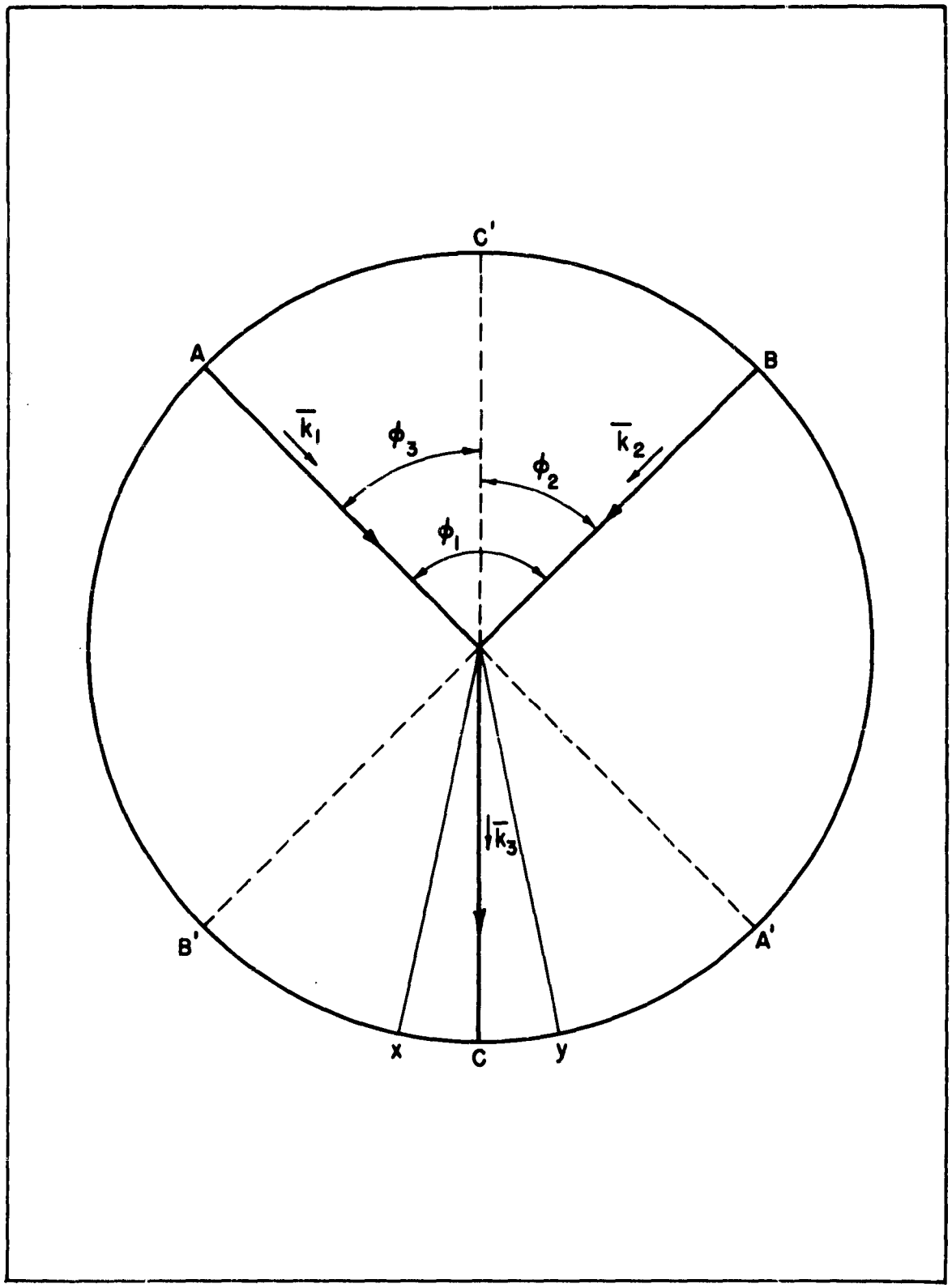

Figure 14 - Disk Shaped Specimen for Study of Ultrasonic Beam Interaction

Another experiment was performed on a magnesium disk to further explore the collimation characteristics of the scattered wave. An additional flat was prepared on either side of position C such that their normals were ±12° from that represented by $\bar{k}_3$ in Figure 14. Although a relatively strong signal was observed at C (on a 6-in. diameter disk), no signals at all were detected at X or Y. These results definitely rule out the possibility that the scattered signals we observe are due to independent scattering of the two primary beams from grain boundaries with subsequent "mixing" of these signals at the receiving transducer. Such scattering would not be particularly directive and produce such a high degree of collimation. The relatively sharp collimation also suggests that the scattered wave is nearly plane and probably suffers less than the R^{-1} fall-off assumed in calculating the amplitude factors of Appendix A.

The relative intensities of the primary and scattered waves have been examined but current results are only qualitative. Generally, the voltages measured on the receiving transducers are 40 - 60 db below those produced by primary wave echos returning to the transmitting crystals.

We have also been interested in measuring changes in the primary beam intensities caused by interaction effects. As discussed in Section IV-A, the intensity of both primary beams might be expected to decrease in those interaction cases where the scattered wave is a sum frequency. In the case of difference frequencies, however, the intensity of the "splitting" wave would be expected to decrease while the other would increase. Experimental efforts to observe these relatively small changes in primary beam intensities have thus far yielded negative results.

Although the intensity curves show that beam interaction should be relatively great in polystyrene, we have been unable to observe a scattered wave in this material. These results can probably be explained by the large ultrasonic attenuation exhibited by polystyrene. A high attenuation will seriously reduce the intensity of the primary beams at the point of intersection as well as quickly attenuate the scattered wave after generation.

V. VISUALIZATION OF ULTRASONIC WAVE PACKETS

A. Instrumentation

The early attempts to detect scattered waves created by beam interactions were confined to the use of transducers. These transducers are quite sensitive to weak signals, but at high frequencies they are highly directive. It was felt that the negative results which came first were possibly due to

slight errors in the calculated propagation direction of the scattered wave. The transducer directivity might therefore prevent detection of the scattered wave. The search for a less directive detector finally led us into various optical techniques. Although these techniques are limited to transparent solids, they do have certain advantages for studying beam interaction. Several waves traveling in different directions can be visualized at the same time and yet the sensitivity of detecting one wave in relation to another may be adjusted.

A simple schematic of our optical detection system is shown in Figure 15. It is basically a standard schlieren system except that modifications have been included to permit the use of polarization techniques. When operated as a simple schlieren system, the polaroids, P and A , will be removed. The xenon flashtube, F , produces a rather fuzzy line source that is imaged on an adjustable slit, S . The light passing through the slit is collected by the lens, L_1 , and converted into a parallel beam. The beam passes through the test block, M , and then into lens, L_2 , which produces a real image of the slit source S at S' . A "stop" is normally positioned at S' to intercept the image of the slit. However, ultrasonic waves in the test block may produce localized gradients in the index of refraction. These gradients, when normal to the optic axis, cause some of the light passing through M to be scattered out of the parallel beam. These rays pass by the stop as illustrated by the dashed lines and are focused onto a ground glass plate or film at G . The regions in the test block where refractive index gradients exist will therefore appear as bright areas on a dark field. When a slit source is used, maximum sensitivity of detecting waves is achieved when the wave front is parallel to the slit. This factor can be used in interaction experiments to accentuate the image of the scattered wave over that of the primary waves.

When the polarizer, P , and analyzer, A , are used as shown in Figure 15, the stop S' is not necessary. If P and A are "crossed," the image at G will generally be a uniform dark field. An ultrasonic wave in the test block M , however, may "depolarize" the parallel beam and thus permit some light to pass through the analyzer. The location of waves will appear as bright areas on a dark field. Weeks[8] has shown that the emergent light intensity is greatest for a longitudinal mode when the plane of polarization of the incident light is inclined at 45° to the direction of sonic propagation. The modulation vanishes when the plane of polarization is parallel or perpendicular to the direction of sonic propagation. Just the opposite is true for transverse waves.

In an experiment in which we wish to detect a relatively weak wave generated at the intersection of two stronger waves, the use of continuously generated waves is prohibited. It would be very difficult indeed to absorb

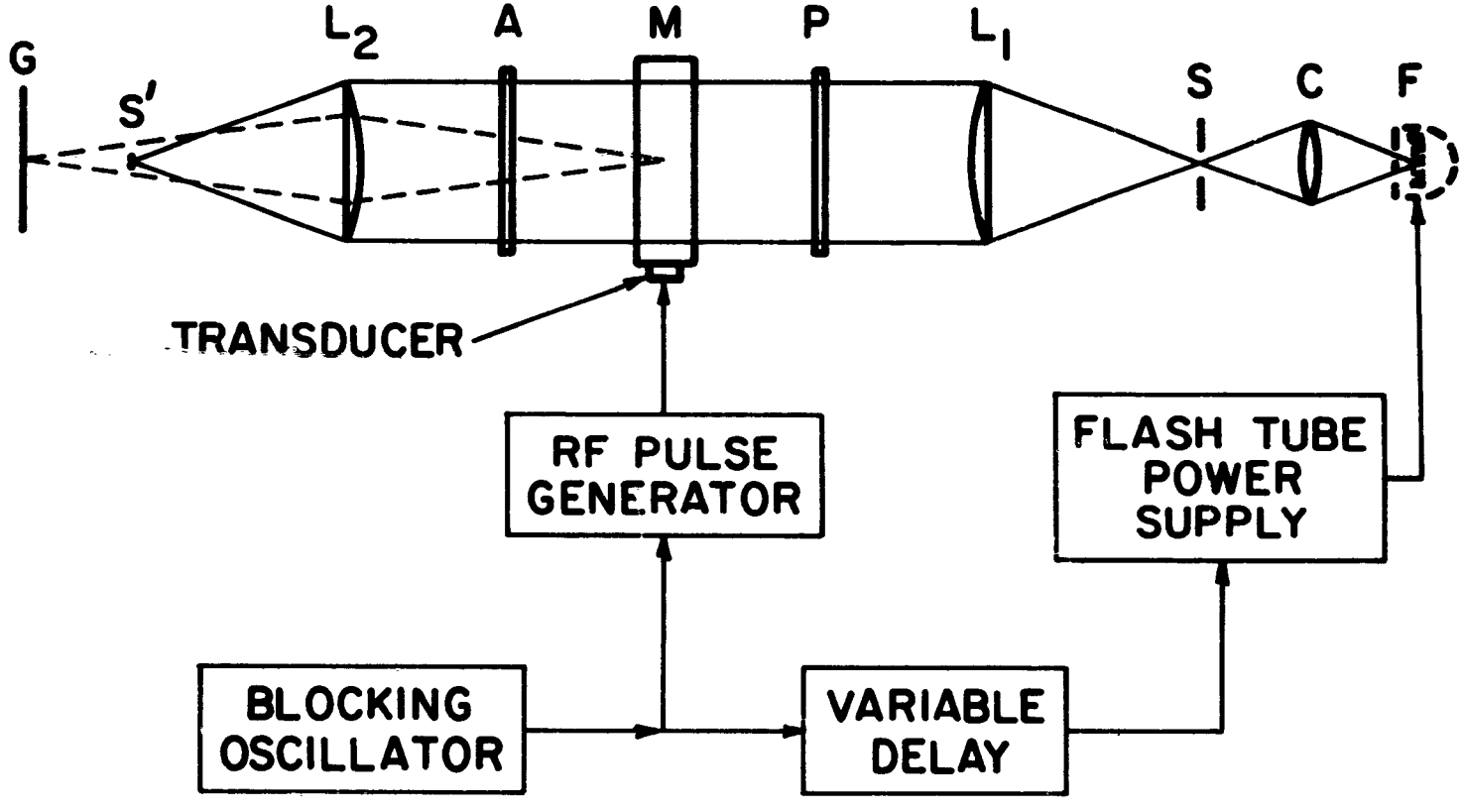

Figure 15 - Optical System for the Observation of Ultrasonic Wave Packets

all of the energy in the primary waves before it is repeatedly reflected at surface boundaries. The reflected waves would ultimately produce index gradients over the entire specimen that would probably be larger than those produced by the scattered wave. This difficulty can be largely overcome by using pulsed ultrasonic waves and a pulsed light source for the optical system.

The blocking oscillator controls the repetition rate of both the rf pulse generator and the pulsing of the light source. However, a variable delay between the blocking oscillator and the flashtube power supply makes it possible to observe the wave packet after it travels a given distance into the test specimen. With a given delay between the pulsing of the ultrasonic generator and the flashtube, one can "stop" the traveling packets at a given position and visually observe or photograph the resultant patterns. A General Radio "Strobotac" was used as the flashtube power supply. The FX-31 xenon flashtube (Edgerton, Germeshausen, and Grier, Inc.) has an optical window which facilitates imaging of the rather fuzzy line source, and it can be flashed at rather high repetition rates.

B. Photographic Results

Figure 16 is a sequence of photographs showing a 7-mc. shear wave packet at various stages of travel in a glass specimen. Standing waves are clear in (c) due to superposition of the incident and reflected traveling waves. Side lobes have developed in (d) as the packet travels back toward the transducer. Figure 17 shows two 7-mc. shear beams intersecting at approximately 90°. Interference between the two beams is easily seen even in areas outside the region of main lobe overlap. The duration of the light pulse in both figures was 0.8 μsec corresponding to a shear wave travel distance of approximately 2 mm.

During the past year, beam interactions were studied simultaneously using both transducers and the optical system. Successful detection of the sought-after beams using transducer techniques lessened our immediate interest in optical techniques. Further experimentation was therefore delayed until more information on the interaction process could be collected. The preliminary results obtained with transducers now suggest that under ideal conditions one should be able to detect the scattered waves with an optical system. Further work along this line is warranted because of the versatility of the optical system in studying beam spreading and structure variations as the scattered waves propagate away from the point of origin.

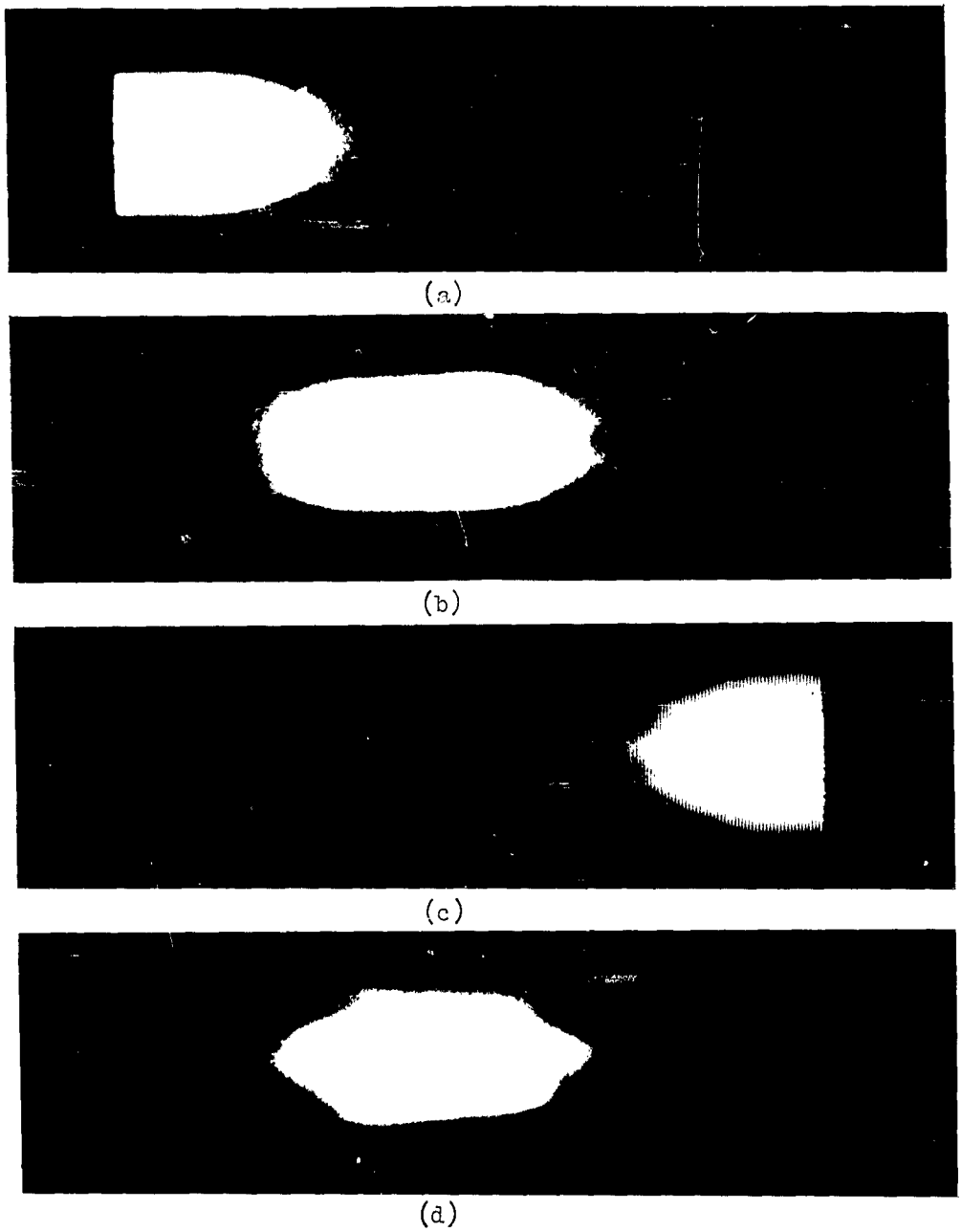

Figure 16 - Sequence of Photographs Showing Ultrasonic Pulse Traveling Through Glass Specimen

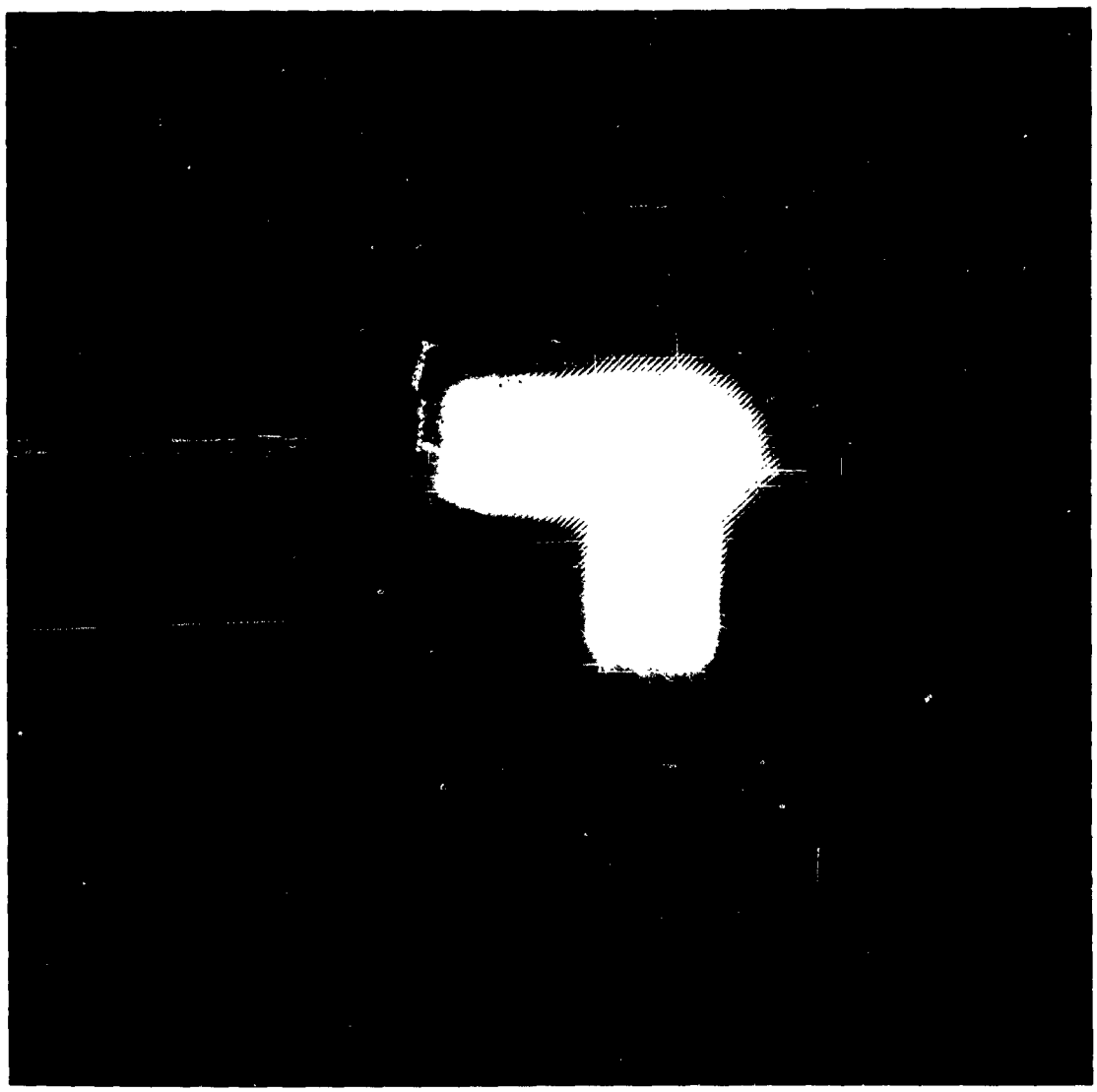

Figure 17 - Intersection of Two 7-mc. Shear Wave Packets in a Glass Specimen

VI. THREE-DIMENSIONAL STRESS ANALYSIS WITH ULTRASONICS

The successful generation and detection of scattered beams of reasonable intensity provides us with a theoretically possible technique of performing three-dimensional stress measurements. Note in Table 1 that a transverse scattered wave can be generated in either case II or case III. For simplicity, let us consider only case II where the interaction of two longitudinal waves may produce a transverse wave of difference frequency. It can be shown theoretically (and confirmed experimentally) that the polarization of the transverse wave lies in the plane defined by the propagation vectors of the two primary waves. We therefore have a potential technique of generating transverse waves of known polarization at any subsurface volume element.

Incorporation of beam interaction techniques into a possible method of three-dimensional stress analysis is illustrated in Figure 18. Primary beams $\bar{k}_1$ and $\bar{k}_2$ are first crossed at position (a) to produce a transverse wave $\bar{k}_3$. With a detector at position (c), the total angular rotation α of the polarization axis, can be determined for propagation between (a) and (c). The primary waves can then be crossed at (b) and the rotation β determined for path (bc). The difference between the secondary principal stresses (in a plane perpendicular to $\bar{k}_3$) can then be approximated for a point midway between (a) and (b). The approximation should take the form

$$(p-q) = K(\alpha-\beta)\ell$$

where p and q are the secondary principal stresses, K is the stress-rotation constant for the material in question and ℓ is the distance between (a) and (b). Since the direction $\bar{k}_3$ and its polarization can be varied through control of $\bar{k}_1$ and $\bar{k}_2$, it should be possible to determine the directions of p and q and the value $(p-q)$ for several different $\bar{k}_3$ directions passing through a common point.

There are many practical problems to be solved before the above procedure will yield much useful information. On certain geometric shapes these problems will be much more severe than others. The difficulty of varying the direction of $\bar{k}_1$ and $\bar{k}_2$ and accurately controlling the intersection point is indeed great, especially in irregularly shaped specimens. However, liquid coupling techniques may prove satisfactory in many cases and thus increase versatility over contact bonding. At any rate, the potential applications of beam scattering techniques in the measurement of stress and other subsurface properties are numerous and deserve considerable attention. Additional work should be directed toward the evaluation of all influencing factors as well as the development of techniques that will facilitate the application to practical problems.

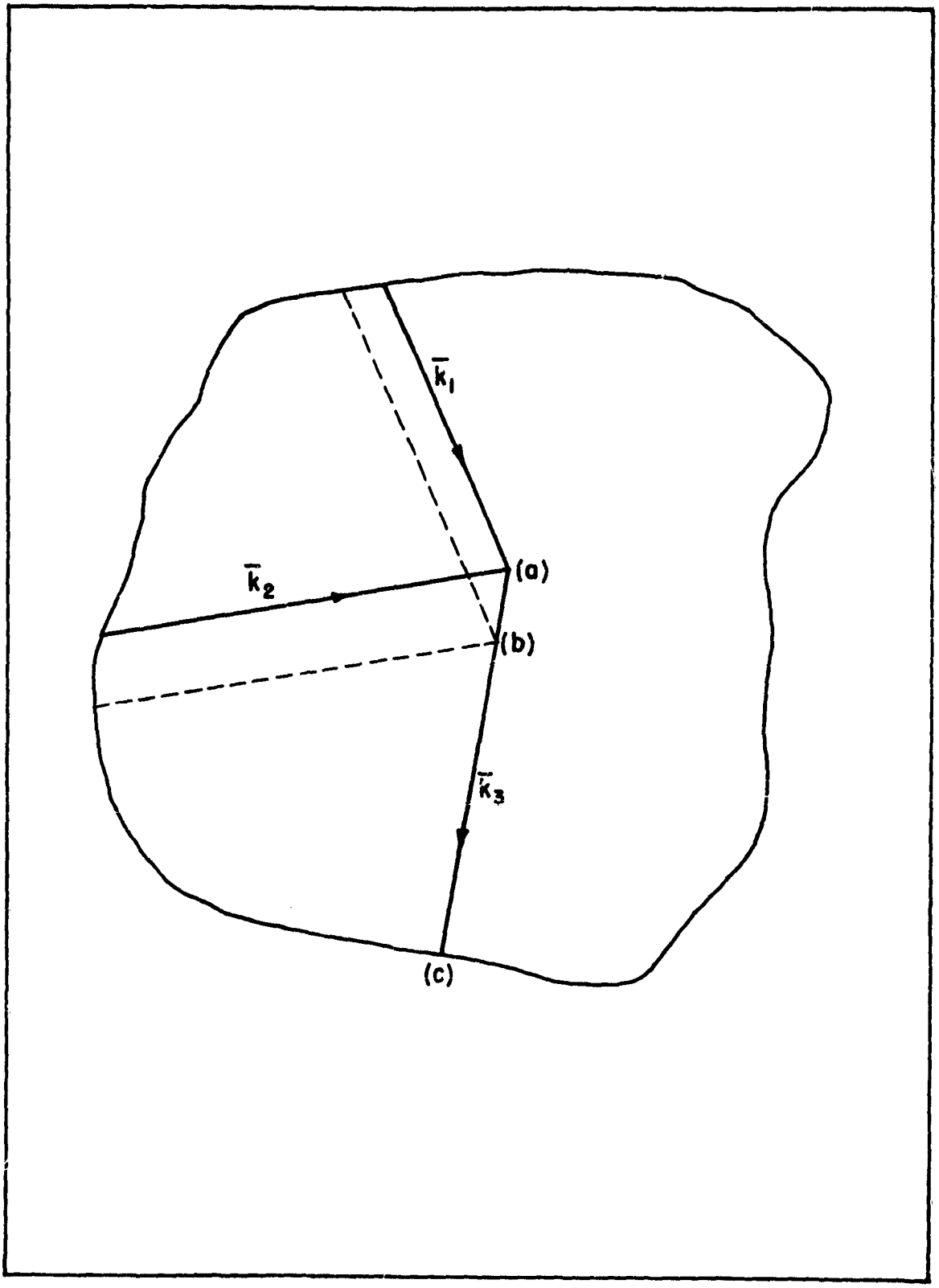

Figure 18 - Schematic Diagram of Potential Stress Analysis Technique Using Beam Interaction to Produce Shear Waves

APPENDIX A

AMPLITUDE EXPRESSIONS FOR SCATTERED WAVES

In the amplitude expressions, the terms are defined as follows:

X_1 , X_2 - amplitudes of primary waves

V - volume of intersection

ω - angular frequency

ρ - density

R - distance between point of intersection and point of observation

c_t - velocity of shear wave

c_ℓ - velocity of longitudinal wave

c - ratio of velocities $\frac{c_t}{c_\ell}$

μ - shear modulus

K - bulk modulus

a - ratio of primary frequencies $\frac{\omega_2}{\omega_1}$

A , B - third order elastic constants

ϕ - angle between primary waves

$\bar{k}_1$, $\bar{k}_2$ - propagation vectors for primary waves

Case I - Two Transverse Waves Interacting to Produce a Scattered Longitudinal Wave of Frequency $(\omega_1+\omega_2)$

(A) Both transverse waves polarized perpendicular to the $\bar{k}_1\bar{k}_2$ plane.

$$\text{amp} = \frac{X_1X_2V\omega_1^3}{16\,\pi\rho R\,c_t^4\,c_\ell}\left\{-\left(\mu+\frac{A}{4}\right)\left[(c^2-1)(a^3+1)+(a^2+a)(c^2+1)\right]\right.$$
$$\left.-\left(K+\frac{\mu}{3}+\frac{A}{4}+B\right)\left[c^2(3c^2-1)(a^2+a)+c^2(c^2-1)(a^3+1)\right]\right\}$$

(B) Both transverse waves polarized in the $\bar{k}_1\bar{k}_2$ plane.

$$\text{amp} = \frac{-X_1X_2V\omega_1^3}{8\,\pi\rho R\,c_t^4\,c_\ell}\left\{ac^2(1+a)\left[-\left(\mu+\frac{A}{2}+B\right)+\cos^2\phi\left(\frac{7}{3}\,\mu+A+K+2B\right)\right]\right\}$$

(C) One transverse wave polarized in $\bar{k}_1\bar{k}_2$ plane and one perpendicular to $\bar{k}_1\bar{k}_2$ plane.

$$\text{amp} = 0$$

Case II - Two Longitudinal Waves Interacting to Produce a Scattered Transverse Wave of Frequency $(\omega_2-\omega_1)$

$$\text{amp} = \frac{-X_1X_2V\omega_1^3}{8\,\pi\rho R\,c_t^2\,c_\ell^3}\left(\frac{7}{3}\,\mu+A+K+2B\right)\cos\phi\left[-(1+P)\cos\phi(2a^3+2aP)+a^2(1+P)^2+(a^2+P)^2\right]^{\frac{1}{2}}$$

where

$$P = \frac{2a^3+a^4c^2+2a^2c^2-a^4-6a^2+2a+c^2-1}{2(a-1)^2}$$

Case III - One Transverse Wave and One Longitudinal Wave Interacting to Produce A Scattered Longitudinal Wave of Frequency $(\omega_1+\omega_2)$

(A) If the transverse wave is polarized in the $\bar{k}_1\bar{k}_2$ plane.

$$\text{amp} = \left(\frac{-X_1X_2V\omega_1^3}{8\,\pi\rho R\, c_t^3\, c_\ell^2}\right)\left[\frac{a(1-\cos^2\phi)^{\frac{1}{2}}}{1+a}\right]\left\{(3\mu+A+B)ac+\left(K+\frac{\mu}{3}+\frac{A}{2}+2B\right)c^2(1+a)^2\cos\phi\right.$$

$$\left.+\left(\frac{13}{3}\mu+\frac{3}{2}A+2B+K\right)c^2\cos\phi+\left(\mu+\frac{A}{4}\right)(2a^2+4ac\cos\phi)\cos\phi\right\}$$

(B) If the transverse wave is polarized perpendicular to the $\bar{k}_1\bar{k}_2$ plane.

$$\text{amp} = 0$$

Case IV - One Transverse Wave and One Longitudinal Wave Interacting to Produce A Scattered Longitudinal Wave of Frequency $(\omega_1-\omega_2)$

(A) If the transverse wave is polarized in the $\bar{k}_1\bar{k}_2$ plane.

$$\text{amp} = \left(\frac{-X_1X_2V\omega_1^3}{8\,\pi\rho R\, c_t^3\, c_\ell^2}\right)\left[\frac{a(1-\cos^2\phi)^{\frac{1}{2}}}{1-a}\right]\left\{\left(3\mu+\frac{A}{2}-B\right)ac\right.$$

$$\left.+\left(\frac{\mu}{3}+K+\frac{A}{2}+2B\right)c^2(1-a)^2\cos\phi-\left(\frac{13}{3}\mu+A+K\right)c^2\cos\phi+\left(\mu+\frac{A}{4}\right)4ac\cos\phi-2a^2)\cos\phi\right\}$$

(B) If the transverse wave is polarized perpendicular to the $\bar{k}_1\bar{k}_2$ plane.

$$\text{amp} = 0$$

Case V - One Transverse Wave and One Longitudinal Wave Interacting to Produce A Scattered Transverse Wave of Frequency $(\omega_1-\omega_2)$

(A) If the primary transverse wave is polarized perpendicular to the $\bar{k}_1\bar{k}_2$ plane.

$$\text{amp} = \left(\frac{X_1X_2V\omega_1^3}{16\,\pi\rho R\, c_t^4\, c_\ell}\right)\frac{1}{c^2}\left\{\left(K+\frac{4}{3}\mu+\frac{A}{2}+B\right)(2ac^2+c^4-c^2)\right.$$
$$\left. -\left(\mu+\frac{A}{4}\right)(4a^2+c^4-2c^2+1+4ac^2-4a)\right\}$$

(B) If the primary transverse wave is polarized in the $\bar{k}_1\bar{k}_2$ plane.

$$\text{amp} = \frac{\omega_1 V}{4\,\pi\rho R\, c_t^2\, c_\ell}\left\{M_1^2+\frac{a^2}{c^2}M_2^2+2M_1M_2\frac{a}{c}\cos\phi\right\}^{\frac{1}{2}}$$

where

$$M_1 = \left\{\frac{D_1-(D_2-D_1)ac\cos\phi+c^2D_1-a^2D_2}{(1-a)^2}\right\}$$

$$M_2 = \left\{\frac{D_2+(D_2-D_1)ac\cos\phi+c^2D_1-a^2D_2}{(1-a)^2}\right\}$$

$$D_1 = \frac{X_1X_2\omega_1^2}{2\,c_t^2(1-\cos^2\varphi)^{\frac{1}{2}}}\left\{2\left(\mu+\frac{A}{4}\right)\left[a^2(2\cos^2\phi-1)-ac\cos^3\phi\right]+\left(\frac{2}{3}\mu-K-B\right)ac\cos\phi\right\}$$

$$D_2 = \frac{X_1X_2\omega_1^2}{2c\,c_\ell^2(1-\cos^2\phi)^{\frac{1}{2}}}\left\{-2\left(\mu+\frac{A}{4}\right)a\cos^3\phi+\left(K+\frac{A}{2}+\frac{\mu}{3}+2B\right)c\cos^2\phi+(\mu-B)c\right\}$$

Always use the positive root of $(1-\cos^2\phi)^{\frac{1}{2}}$.

BIBLIOGRAPHY

1. F. R. Rollins, "Ultrasonic Methods for Nondestructive Measurement of Residual Stress," WADD TR 61-42, Part I (1961).

2. F. R. Rollins, "Ultrasonic Methods for Nondestructive Measurement of Residual Stress," WADD TR 61-42, Part II (1962).

3. M. M. Frocht and L. S. Srinath, Proc. Third U. S. National Congress of Applied Mechanics, 329 (1958).

4. E. G. Coker,and L. N. G. Filon, "A Treatise on Photoelasticity," second edition, p. 410 (Cambridge University Press, 1957).

5. G. L. Slonimskii, J.E.T.P. (U.S.S.R.) 12, 1457 (1937).

6. D. S. Hughes and J. L. Kelly, Phys. Rev., 92, 1145 (1953).

7. A. Seeger and O. Buck, Z. Naturforschung, 15a, 1056 (1960).

8. R. F. Weeks, J.A.S.A., 33, 741 (1961).

Aeronautical Systems Division, Dir/Materials and Processes, Nonmetallic Materials Lab., Wright-Patterson AFB, Ohio.
Rpt No. WADD TR 61-42, Pt III, STUDY OF ULTRASONIC TECHNIQUES FOR THE NONDESTRUCTIVE MEASUREMENT OF RESIDUAL STRESS, Final Report, May 63, 39p., incl. illus., tables and 8 refs.

Unclassified Report

The theoretical and experimental investigation of ultrasonic beam interaction in solid materials has been continued. Interaction of pulsed beams (3-15 mc/s) under "resonant"

(over)

conditions reveals that interaction does occur in many materials. A theoretically predicted third beam is generated at the "point" of intersection and has been experimentally observed in samples of fused silica, polycrystalline aluminum, and polycrystalline magnesium. A potential method of three-dimensional stress analysis is discussed. An optical system for studying beam interaction in transparent solids is also described.

1. Methods, ultrasonic
2. Stresses, residual
I. AFSC Project 7360, Task 73606
II. Contract No. AF 33(616)-7058
III. Midwest Research Institute, Kansas City, Missouri
IV. Rollins, Fred R., Jr. Waldow, Peter
V. Aval fr OTS
VI. In ASTIA collection

Aeronautical Systems Division, Dir/Materials and Processes, Nonmetallic Materials Lab., Wright-Patterson AFB, Ohio.
Rpt No. WADD TR 61-42, Pt III, STUDY OF ULTRASONIC TECHNIQUES FOR THE NONDESTRUCTIVE MEASUREMENT OF RESIDUAL STRESS, Final Report, May 63, 39p., incl. illus., tables and 8 refs.

Unclassified Report

The theoretical and experimental investigation of ultrasonic beam interaction in solid materials has been continued. Interaction of pulsed beams (3-15 mc/s) under "resonant"

(over)

conditions reveals that interaction does occur in many materials. A theoretically predicted third beam is generated at the "point" of intersection and has been experimentally observed in samples of fused silica, polycrystalline aluminum, and polycrystalline magnesium. A potential method of three-dimensional stress analysis is discussed. An optical system for studying beam interaction in transparent solids is also described.

1. Methods, ultrasonic
2. Stresses, residual
I. AFSC Project 7360, Task 73606
II. Contract No. AF 33(616)-7058
III. Midwest Research Institute, Kansas City, Missouri
IV. Rollins, Fred R., Jr. Waldow, Peter
V. Aval fr OTS
VI. In ASTIA collection